Available on the CERN CDS information server **CMS PAS SUS-13-020**

CMS Physics Analysis Summary

Contact: cms-pag-conveners-susy@cern.ch 2014/04/03

Phenomenological MSSM interpretation of the CMS 7 and 8 TeV results

The CMS Collaboration

Abstract

We interpret within the phenomenological MSSM (pMSSM) results from searches for new physics performed by CMS in pp data sets collected at 7 TeV and 8 TeV, corresponding to integrated luminosities of 5 fb^{-1} and 19.5 fb^{-1}, respectively. The pMSSM is a 19-parameter realization of the MSSM, defined at the SUSY scale, that captures most of the features of the general R-parity conserving weak-scale MSSM. It allows us to draw conclusions that are more generic than , and complimentary to, those derived in more constrained models, including simplified models and those that impose particular SUSY breaking schemes, such as the CMSSM. We perform a global Bayesian analysis on a data set, which in addition to CMS search results, includes data from pre-CMS and indirect measurements. We study posterior probability densities of model parameters, masses and observables and study implications for the MSSM Higgs sector and dark matter searches. Our study provides a coherent global picture of how the current CMS searches constrain supersymmetry in general.

Contents

1 Introduction

The recent discovery [1, 2] of a Higgs-boson-like particle is clearly the most significant news from the Large Hadron Collider (LHC). The other significant news from the LHC is the absence of any compelling sign of new physics. In particular, there is no hint of supersymmetry (SUSY), one of the most thoroughly studied ideas for physics beyond the Standard Model (BSM) (see, for example, Refs. [3, 4] for recent reviews).

The absence of evidence, however, may not be evidence of absence. Searches for SUSY have typically been interpreted within constrained models with just a few parameters. A commonly used model is the Constrained Minimal Supersymmetric Standard Model (CMSSM), which is characterized by four parameters and a sign [5–11]: a universal scalar mass m_0, a gaugino mass $m_{1/2}$ and a trilinear coupling A_0 defined at the GUT scale, $M_{\rm GUT} \sim 10^{16}$ GeV, together with $\tan\beta$ and sign(μ). The simplifying assumption of universality at the GUT scale has served a useful purpose: for many years it has provided a framework for gauging progress in SUSY searches. However, many mass patterns and signatures that are *a priori* possible in the MSSM cannot be realized in the CMSSM. Therefore, interpreting the experimental results only in the $(m_0, m_{1/2})$ plane carries the risk of imposing overly strong constraints on SUSY that are not warranted by observations. The full set of mass patterns and signatures possible in the MSSM are also not necessarily accounted for in the Simplified Model Spectra (SMS) [12–14] approach. Although interpretation using SMS topologies is very useful since it allows us to systematically see the experimental impact on well-defined, isolated topologies, it is crucial to complement this by interpretation within a generic model, such as the phenomenological MSSM (pMSSM) [15], that intrinsically covers a wide diversity of topologies. Of course, it is also possible that the SMS approach eliminates a pMSSM parameter point that is not eliminated in the present version of the analysis presented here if the latter set of analyses does not include some important channel/configuration considered by the SMS analyses. The SMS approach and the pMSSM approach become equivalent only when: a) the set of analyses in the pMSSM approach is the same as the set of analyses considered in the simplified models; and b) the simplified models cover all the final states to which these analyses can be sensitive for each pMSSM point.

In order to be more general, *i.e.*, to account fully for the plethora of mass patterns and decay modes that can occur in the MSSM, it is necessary to pursue a less model-dependent ap-

proach. In this paper we therefore use the pMSSM, a 19-dimensional realization of the MSSM, which captures most of the phenomenological features of the R-parity conserving MSSM. In the pMSSM, all MSSM parameters are specified at the electroweak scale and allowed to vary freely subject to the requirement that the model be consistent with electroweak symmetry breaking and other such basic constraints. Since the pMSSM includes neither relations between SUSY breaking terms at a high scale, nor large correlations between sparticle masses from renormalization group evolution, it allows a much broader set of scenarios than those in, e.g., the CMSSM and related GUT-scale models. Many of these are difficult to constrain using current LHC data — in particular, scenarios with much lower SUSY masses can evade detection.

To assess what the data obtained by CMS do and do not tell us about SUSY in the context of the pMSSM we use a representative subset of the results obtained by CMS corresponding to integrated luminosities of 5 fb^{-1} at 7 TeV and 19.5 fb^{-1} at 8 TeV. The current study extends our analysis [16] of the 7 TeV data. We work within a subspace of the pMSSM where the chargino lifetime $c\tau(\tilde{\chi}_1^{\pm})$ is less than 10 mm to look at the class of final states with prompt decays. In order to combine both data sets we use the same model points within the pMSSM parameter space, chosen randomly from a scan of points consistent with basic constraints and treat the 7 TeV and 8 TeV data in an entirely parallel fashion. The approach employed is an extension of the pioneering work of Ref. [17], which interpreted three independent CMS analyses based on 1 fb^{-1} of CMS data [18–20] in terms of the pMSSM, confirming that the approach is both feasible and better at obtaining general conclusions about supersymmetry than those based on constrained SUSY models. Note that the diversity of phenomena covered by the pMSSM is also helpful in suggesting new approaches to searching for SUSY at the LHC.

As in Ref. [16], the present study follows closely the Bayesian approach (see for example [21, 22]) of Ref. [17]. Prior to this work, the parameter space of the pMSSM and the various LHC constraints on it were studied in detail in Refs. [23–34].

The paper is organized as follows. The definition of the pMSSM is given in Section 2. It is followed by the description of our analysis in Section 3, which includes the construction of the model prior in Section 3.1, and the calculation of the CMS likelihoods in Section 3.2.2. Our results are presented in Section 4, including discussions of the impact of the CMS searches and their current sensitivity to the pMSSM. Section 5 contains our conclusions.

2 Definition of the Phenomenological MSSM

A priori, the weak-scale MSSM has 120 free parameters, assuming that *R*-parity is conserved (to avoid proton decay and to ensure that the lightest SUSY particle, the LSP, is stable) and assuming that the gravitino is heavy. This is clearly too much for any phenomenological study. However, most of these parameters are associated with CP-violating phases and, or, flavor changing neutral currents (FCNC), which are severely constrained by experiment. A few reasonable assumptions about the flavor and CP structure therefore allow us to reduce the number of free parameters by a factor 6, without imposing any SUSY breaking scheme. Working with parameters defined at the weak scale is indeed of great advantage for our purpose because models of SUSY breaking always introduce relations between the soft terms that need not hold in general.

Concretely, the only generic way to satisfy very strong constraints on CP violation is to take all parameters to be real. FCNC constraints are satisfied in a comprehensive way by taking all sfermion mass matrices and trilinear couplings to be flavor-diagonal. Moreover, the first two generations of sfermions are taken to be degenerate. Regarding the trilinear A-terms of

the first two generations, these only enter phenomenology multiplied by the associated very small Yukawa couplings and are thus not experimentally relevant. Only the 3rd generation parameters A_t, A_b and A_τ have consequences that are potentially observable.

This leaves us with 19 real, weak-scale SUSY Lagrangian parameters, the so-called pMSSM [15]. As mentioned, the pMSSM captures most of the phenomenological features of the R-parity conserving MSSM and, most importantly, encompasses and goes beyond a broad range of more constrained SUSY models. The free parameters of the pMSSM are the following:

- three independent gaugino mass parameters M_1, M_2, and M_3,
- the ratio of the Higgs vacuum expectation values (VEV) $\tan\beta = v_2/v_1$,
- the higgsino mass parameter μ and the pseudo-scalar Higgs boson mass m_A,
- 10 (independent) sfermion mass parameters $m_{\tilde{F}}$, where $\tilde{F} = \tilde{Q}_1$, $\tilde{U}_1$, $\tilde{D}_1$, $\tilde{L}_1$, $\tilde{E}_1$, $\tilde{Q}_3$, $\tilde{U}_3$, $\tilde{D}_3$, $\tilde{L}_3$, $\tilde{E}_3$ (and for the 2nd generation we take $m_{\tilde{Q}_2} = m_{\tilde{Q}_1}$, $m_{\tilde{L}_2} = m_{\tilde{L}_1}$, $m_{\tilde{U}_2} = m_{\tilde{U}_1}$, $m_{\tilde{D}_2} \equiv m_{\tilde{D}_1}$, and $m_{\tilde{E}_2} \equiv m_{\tilde{E}_1}$), and
- the trilinear couplings A_t, A_b and A_τ ,

in addition to the standard model parameters. To minimize theoretical uncertainties in the Higgs sector, these parameters are conveniently defined at the scale, $M_{\text{SUSY}} \equiv \sqrt{m_{\tilde{t}_1} m_{\tilde{t}_2}}$, often also referred to as the electroweak symmetry breaking (EWSB) scale.

The pMSSM parameter space is constrained by a number of theoretical requirements. First, the sparticle spectrum must be free of tachyons and cannot lead to color or charge breaking minima in the scalar potential. We also require that EWSB be consistent and that the Higgs potential be bounded from below. Finally, in this study, we also require that the LSP be the lightest neutralino, $\tilde{\chi}_1^0$. This leaves us with a model that is an excellent proxy for the full MSSM with a sufficiently small number of parameters such that a complete exploration of it is possible given existing computer resources.

Interesting to note are the generic properties of sparticle mass spectra of pMSSM scenarios. By definition, each first generation sfermion is exactly degenerate in mass with the corresponding second generation sfermion. Other generic properties of pMSSM mass spectra are actually MSSM properties: In the first and second generation, spartners of left-handed down-type quarks are strongly mass-degenerate with the corresponding up-type squarks. Likewise, first and second generation spartners of left handed charged leptons are strongly degenerate with the corresponding sneutrinos. Usual pMSSM scenarios have three groups of strongly mass degenerate charginos and neutralinos: a first group consists of two neutralinos and one chargino that are fairly pure higgsino states, the second group consists of two neutralinos that are farily pure bino states, while the third group consists of one neutralino and one chargino that are both fairly pure wino states.

3 Analysis

The purpose of this study is to assess what current data tell us, and do not tell us, about the MSSM using the more tractable pMSSM as a proxy. Using these data we perform a global Bayesian analysis that yields posterior probability densities of model parameters, masses, and observables.

3.1 Construction of the pMSSM prior

We work within the sub-space,

$$\begin{gathered}
-3\,\text{TeV} \leq M_1, M_2 \leq 3\,\text{TeV} \\
0 \leq M_3 \leq 3\,\text{TeV} \\
-3\,\text{TeV} \leq \mu \leq 3\,\text{TeV} \\
0 \leq m_A \leq 3\,\text{TeV} \\
2 \leq \tan\beta \leq 60 \\
0 \leq \tilde{Q}_{1,2}, \tilde{U}_{1,2}, \tilde{D}_{1,2}, \tilde{L}_{1,2}, \tilde{E}_{1,2}, \tilde{Q}_3, \tilde{U}_3, \tilde{D}_3, \tilde{L}_3, \tilde{E}_3 \leq 3\,\text{TeV} \\
-7\,\text{TeV} \leq A_t, A_b, A_\tau \leq 7\,\text{TeV},
\end{gathered} \tag{1}$$

of the pMSSM parameters described in Section 2 and the unbounded SM sub-space defined by m_t, $m_b(m_b)$, and $\alpha_s(M_Z)$. We use a likelihood that includes a part that constrains the SM parameters. A point in this space will be denoted by θ. The sub-space defined in Eq. (1) was chosen to be large enough to cover the range of sparticle masses to which the LHC might conceivably be ultimately sensitive. The lower bound of 2 for $\tan\beta$ was chosen in order to avoid any issues of non-perturbativity for the top-quark Yukawa coupling after evolution up to the GUT scale. Typically, perturbativity becomes a very serious issue for $\tan\beta \lesssim 1.7$.

Given a point θ in pMSSM parameter space, masses and observables are calculated as follows. The physical masses and interactions are calculated to state-of-the-art accuracy, using `SoftSUSY_3.3.1` [35] as the spectrum generator, with the input parameters defined at M_{SUSY}. Thus the spectrum calculation includes 1-loop corrections for sparticle masses and mixings, as well as 2-loop corrections for the light Higgs boson mass. Low-energy constraints are calculated with `SuperIso_v3.3` [36], and `micrOMEGAs_2.4.5` [37–39] is used to compute the dark matter relic density $\Omega_{\tilde{\chi}_1^0}h^2$, direct detection cross sections, and to check compatibility with various pre-LHC sparticle mass limits. Moreover, we use SDECAY1.3 [40] to calculate sparticle decay tables and HDECAY5.11 [41] to calculate Higgs boson decay tables. The various codes are interfaced using the SUSY Les Houches Accord [42].

We start the inference chain from a flat initial prior, $p_0(\theta) = \text{constant}$[1]. The theoretical requirements listed at the end of Section 2 are imposed by multiplying this initial prior with a binary probability density function, $p(\text{theory}|\theta)$, which takes value 1 for pMSSM points that meet the requirements and value 0 otherwise. In the same fashion we impose a model constraint on the lifetime of charginos, $c\,\tau(\tilde{\chi}_1^\pm) < 10$ mm with a binary probability density function $p(\text{prompt}\ \tilde{\chi}^\pm|\theta)$. This constraint was introduced because the fast detector simulation used to model the detector response for signal events, described in Section 3.2.2, does not provide a proper description of long-lived charginos. As such we arrive at a prior of the form

$$p(\theta) = p(\text{prompt}\ \tilde{\chi}^\pm|\theta)\,p(\text{theory}|\theta)\,p_0(\theta). \tag{2}$$

Then, we consider data from indirect measurements and pre-CMS searches, listed in Table 1. We refer to this data as non-DCS data, $D^{\text{non-DCS}}$, since it is not originating from Direct CMS Searches (DCS) for new physics. To avoid making cosmological assumptions, data from dark matter experiments are not included. From the non-DCS data, a non-DCS likelihood is constructed as follows. For each non-DCS datum $D_j^{\text{non-DCS}}$ we introduce a likelihood $L(D_j^{\text{non-DCS}}|\mu_j(\theta))$, listed in Table 1, where $\mu_j(\theta)$ denotes the model prediction for the corresponding observable.

[1] Recently, this prior has been referred to as the *ur-prior* from the German prefix *ur* meaning original or primitive (Glen Cowan).

Since the non-DCS data are independent, the non-DCS likelihood is obtained by multiplying the likelihoods for the different non-DCS data,

$$L(D^{\text{non-DCS}}|\theta) = \prod_j L(D_j^{\text{non-DCS}}|\mu_j(\theta)). \tag{3}$$

When we multiply this likelihood to the prior in Eq. (2), we obtain a distribution that includes the data from non-DCS measurements. In this study, this distribution is used as the prior distribution $p^{\text{non-DCS}}(\theta)$,

$$p^{\text{non-DCS}}(\theta) = L(D^{\text{non-DCS}}|\theta)\, p(\theta). \tag{4}$$

We obtain a discrete representation of the non-DCS prior within the sub-space defined in Eq. (1) using a Markov Chain Monte Carlo (MCMC) method [22, 53–56]. A probability density function $p^{\text{non-DCS}\,*}(\theta)$ is constructed including the initial flat prior, the binary likelihood imposing the theoretical constraints, and likelihoods for measurements 1a, 2a, 3a, 4, 5a, 6, 7, 8a, and 9 in Table 1. Approximately 20 million points are sampled from this probability density function within the pMSSM sub-space, using multiple MCMC chains. By construction, this method produces a sample of points whose density in the neighborhood of any θ in the pMSSM sub-space is $\propto p^{\text{non-DCS}\,*}(\theta)$. During the course of this study, measurements on $BR(b \to s\gamma)$, $BR(B_s \to \mu\mu)$, $R(B_u \to \tau\nu)$, m_t, and m_h were updated. We take the effect of these new measurements (1b, 2b, 3b, 5b, and 8b in Table 1) into account by reweighting each sampled point by the ratio of the likelihood given by the new measurement to the likelihood given by the old measurement for each observable. Finally, the requirement on the lifetime of the chargino is taken into account by further weighting the pMSSM points with value 1 or 0 for scenarios that respectively match or fail this requirement, effectively reducing the number of sampled points by 30%.

The probability distributions of selected pMSSM parameters and sparticle masses after imposing various non-DCS requirements are presented in [16]. Here we provide a brief description. Even before applying the constraints of Table 1, the theoretical constraints listed in the previous section significantly sculpt the initial flat distributions of the pMSSM parameters listed in Eq. (1). In particular: μ, M_1, and M_2 become sharply peaked near 0; large values of M_3 and all soft squark masses are most probable. Correspondingly, the masses of $\widetilde{\chi}_1^0$, $\widetilde{\chi}_2^0$, and $\widetilde{\chi}_1^\pm$ become sharply peaked at low values, $\lesssim$ 100 GeV, while a preference for large values of the gluino and first two generation squark masses emerges. The $\tilde{b}_1$ and $\tilde{t}_1$ distributions have a strong peak in the vicinity of 1 TeV, low and high values being significantly disfavored. All of these features are subject, at least to some extent, to boundary effects. The light Higgs boson mass has small probability outside the 112 GeV $-$ 130 GeV window – indeed, significant probability near $m_h = 125$ GeV is an inherent feature of the pMSSM parameter space once theoretical constraints are imposed.

Some of these features, but not all, are significantly altered when the constraints of Table 1 are added to the theoretical constraints. The peak of M_1 near 0 is increased in strength but the peaks in μ and M_2 near 0 are turned into suppressions, with $|\mu| \sim 300$ GeV and $|M_2| \gtrsim 300$ GeV being strongly preferred. The preference for low values of $\tan\beta$, $\lesssim 25$, is significantly increased, and large $m_{\tilde{Q}_3}$, $\gtrsim$ 1.5 TeV, becomes strongly preferred. As for the sparticle masses, the sharp peak of $m_{\widetilde{\chi}_1^0}$ near 0 is shifted to $\sim 100 - 200$ GeV. One finds that $m_{\widetilde{\chi}_2^0}$ and $m_{\widetilde{\chi}_1^\pm}$ cannot be below 100 GeV (due to LEP data) and peaks emerge in the $200 - 500$ GeV region. The $\tilde{g}$ mass distribution is shifted to somewhat higher values, the $\tilde{u}_R, \tilde{c}_R$ mass distributions are hardly changed, the $m_{\tilde{b}_1}$ distribution is shifted to somewhat higher values. The $m_{\tilde{t}_1}$ distribution is shifted to still higher values, with very little probability below 500 GeV. It is interesting to emphasize that all the above-mentioned shifts already arise as a result of the constraints listed in Table 1, even before

Table 1: The measurements that are the basis of our pMSSM prior $p^{\text{non-DCS}}(\theta)$. All measurements except the measurement of m_h at the LHC were used to sample points from the pMSSM parameter space via Markov Chain Monte Carlo (MCMC). The m_h likelihood was imposed afterwards as a weight on the sampled points. The likelihood for each point was reweighted post-MCMC based on the recent measurements on $BR(b \to s\gamma)$, $BR(B_s \to \mu\mu)$, $R(B_u \to \tau\nu)$ (where $R \equiv BR_{\text{MSSM}}/BR_{\text{SM}}$), and m_t. To the measurement of the anomalous magnetic moment of the muon, an additional uncertainty was added to account for theoretical uncertainties in the SUSY calculations.

i	Observable $\mu_j(\theta)$	Constraint $D_j^{\text{non-DCS}}$	Likelihood function $L(D_j^{\text{non-DCS}}\|\mu_j(\theta))$	MCMC / post-MCMC
1a	$BR(b \to s\gamma)$ [43, 44]	$(3.55 \pm 0.23^{\text{stat}} \pm 0.24^{\text{th}} \pm 0.09^{\text{sys}}) \times 10^{-4}$	Gaussian	MCMC
1b	$BR(b \to s\gamma)$ [45]	$(3.43 \pm 0.21^{\text{stat}} \pm 0.24^{\text{th}} \pm 0.07^{\text{sys}}) \times 10^{-4}$	Gaussian	reweight
2a	$BR(B_s \to \mu\mu)$ [46]	observed CLs curve from [46]	$d(1-CLs)/d(BR(B_s \to \mu\mu))$	MCMC
2b	$BR(B_s \to \mu\mu)$ [47]	$(2.9 \pm 0.7 \pm 0.29^{th}) \times 10^{-9}$	Gaussian	reweight
3a	$R(B_u \to \tau\nu)$[36, 48]	1.63 ± 0.54	Gaussian	MCMC
3b	$R(B_u \to \tau\nu)$[45]	1.04 ± 0.34	Gaussian	reweight
4	Δa_μ [49]	$(26.1 \pm 6.3^{\text{exp}} \pm 4.9^{\text{SM}} \pm 10.0^{\text{SUSY}}) \times 10^{-10}$	Gaussian	MCMC
5a	m_t [50]	$173.3 \pm 0.5^{\text{stat}} \pm 1.3^{\text{sys}}$ GeV	Gaussian	MCMC
5b	m_t [51]	$173.20 \pm 0.87^{\text{stat}} \pm 1.3^{\text{sys}}$ GeV	Gaussian	reweight
6	$m_b(m_b)$ [48]	$4.19^{+0.18}_{-0.06}$ GeV	Two-sided Gaussian	MCMC
7	$\alpha_s(M_Z)$ [48]	0.1184 ± 0.0007	Gaussian	MCMC
8a	m_h	pre-LHC: $m_h^{low} = 112$	1 if $m_h \geq m_h^{low}$ 0 if $m_h < m_h^{low}$	MCMC
8b	m_h	LHC: $m_h^{low} = 120$, $m_h^{up} = 130$	1 if $m_h^{low} \leq m_h \leq m_h^{up}$ 0 if $m_h < m_h^{low}$ or $m_h > m_h^{up}$	reweight
9	sparticle masses	LEP [52] (via micrOMEGAs [37–39])	1 if allowed 0 if excluded	MCMC

imposing 120 GeV $< m_h <$ 130 GeV. In particular, the small probability for $m_{\tilde{t}_1} \lesssim 500$ GeV arises in order to describe the $b \to s\gamma$ observations. Imposing 120 GeV $< m_h <$ 130 GeV has very little additional impact, except to change a moderately flat $|A_t|$ distribution to one with little probability for $|A_t| \lesssim 2$ TeV.

3.2 Construction of CMS posterior distributions

To study the impact of CMS searches on the pMSSM, we compare the non-DCS prior $p^{\text{non-DCS}}(\theta)$, introduced in the previous section with a posterior distribution, $p(\theta|D^{\text{CMS}}))$ including CMS data D^{CMS}. This posterior distribution is constructed by multiplying a CMS likelihood $L(D^{\text{CMS}}|\theta)$ with the non-DCS prior,

$$p(\theta|D^{\text{CMS}}) = L(D^{\text{CMS}}|\theta)p^{\text{non-DCS}}(\theta). \quad (5)$$

The next sections describe which CMS data is considered in this study and how CMS likelihoods are constructed.

3.2.1 CMS analyses included in this study

We list in Table 2 the CMS analyses we have implemented in this study. These analyses, which are a subset of the 7 and 8 TeV CMS searches for new physics, cover a variety of final states.

Table 2: List of CMS analyses included in the CMS likelihood $L(D^{\text{CMS}}|\theta)$. The columns show the analysis names (Analysis), the center-of-mass energy at which data was collected ($\sqrt{s}$), the integrated luminosity to which the data corresponds (L), the likelihood methods used, as defined in Section 3.2.3 and 3.2.4 (Likelihood), and the reference to the analysis documentation (Ref.). For the 8 TeV leptonic search for electroweak (EW) production of $\widetilde{\chi}^0$, $\widetilde{\chi}^{\pm}$, $\tilde{l}$ the included channels are the same sign di-lepton channel (ss), the three lepton channel (3l), and the four lepton channel (4l). For all other analyses, all channels are taken into account.

Analysis	$\sqrt{s}$	L	Likelihood	Ref.
Hadronic HT + MHT search	7 TeV	4.98 fb^{-1}	method 1	[57]
Hadronic HT + MET + b-jets search	7 TeV	4.98 fb^{-1}	method 1	[58]
Leptonic search for EW prod. of $\widetilde{\chi}^0$, $\widetilde{\chi}^{\pm}$, $\tilde{l}$	7 TeV	4.98 fb^{-1}	method 1	[59]
Hadronic HT + MHT search	8 TeV	19.5 fb^{-1}	method 1	[60]
Hadronic HT + MET + b-jets search	8 TeV	19.4 fb^{-1}	method 2	[61]
Leptonic search for EW prod. of $\widetilde{\chi}^0$, $\widetilde{\chi}^{\pm}$, $\tilde{l}$ (ss, 3l, and 4l channels)	8 TeV	19.5 fb^{-1}	method 1	[62]

The goal is to test different regions of the pMSSM parameter space, characterized by different admixtures of final state topologies. The hadronic HT + MHT search is expected to have the greatest sensitivity over the pMSSM space. It is an inclusive analysis based on ≥ 3 jets and missing transverse energy that targets gluino and squark production with long hadronic cascades. The hadronic HT + MET + b-jets search that involves ≥ 3 jets and ≥ 1 b-jet primarily focuses on gluinos decaying to hadronic 3rd generation particles. Finally, the leptonic search for electroweak (EW) production of $\widetilde{\chi}$, $\tilde{e}$, $\tilde{\mu}$ targets neutralino-chargino pair production and slepton pair production with leptonic decays by probing final states with multiple leptons and missing energy. In this study, we present a first combination of the 7 TeV and 8 TeV SUSY results for each of the given three analyses.

3.2.2 CMS likelihoods

To study the impact of CMS searches, a random sub-sample of 7205 points was selected from the set of pMSSM points surviving the post-MCMC requirements, (where surviving requires having weight greater than zero). For each point θ in the sub-sample of 7205 points and for each considered CMS datum $D_l^{\rm CMS}$, we calculate likelihoods $L(D_l^{\rm CMS}|\mu_l(\theta))$, where $\mu_l(\theta)$ denotes the predicted values for the observables associated to $D_l^{\rm CMS}$. We make use of two distinct methods to calculate these CMS likelihoods: For pure count experiments we use "likelihood method 1" described in Section 3.2.3. For analyses that perform a fit on background control regions and signal regions simultaneously, we rely on "likelihood method 2" described in Section 3.2.4. As indicated Table 2, we use method 1 for all analyses except for the 8 TeV HT + MET + b-jets search for which we use method 2.

For both likelihood approaches, the predictions $\mu_l(\theta)$ are obtained from MC simulation: for each pMSSM point θ we generate 10000 signal events using `PYTHIA6` [63] and simulate the response of the CMS detector using a fast simulation [64]. Signal cross sections are calculated at leading order with `PYTHIA6`. Uncertainties on the predictions $\mu_l(\theta)$ are not fully taken into account. Instead we compare results obtained assuming the central signal prediction cross section with results obtained while scaling the signal cross sections up or down by 50%.

A discrete representation of the posterior density $p(\theta|D^{\rm CMS}) \propto L(D^{\rm CMS}|\theta)\, p(\theta)$ is obtained by further weighting each of the selected pMSSM points with $L(D^{\rm CMS}|\theta)$ and subsequent normalization to unity over the pMSSM sub-space given in Eq. (1).

3.2.3 Likelihood method 1

This method is used for pure count experiments. Since the experimental results are event counts, we assume the likelihood to be a Poisson distribution,

$$L(D_l^{CMS}|\mu_l(\theta)) = \text{Poisson}(N_l|s_l(\theta) + b_l), \tag{6}$$

with observed count N_l and expected count $s_l(\theta) + b_l$ ($\equiv \mu_l(\theta)$), where b_l is the expected background count[2] for the $l^{\rm th}$ experimental result and $s_l(\theta)$ is the expected signal count for pMSSM point θ as predicted with MC simulation. In the current study, we neglect the uncertainty on $s_l(\theta)$. In effect, we assume δ-function priors for the expected signals. However, as already mentioned, we repeat the calculations with the predicted signal cross section scaled up or down by $\pm 50\%$.

The information about each background parameter b_l is given by the background estimate B_l and its associated uncertainty δB_l. For the probability density for b_l we assume a gamma distribution,

$$p(b_l|B_l, dB_l) = \text{Gamma}(x; \alpha, \beta), \tag{7}$$

where $\text{Gamma}(x;\alpha,\beta) = \beta \exp(-\beta x)(\beta x)^{\alpha-1}/\Gamma(\alpha)$. We choose α and β such that b_l reaches maximum probability at value B_l and has variance δB_l^2. For each pMSSM point, and for each CMS experimental result, we compute the marginal likelihood

$$p(N_l|s_l(\theta)) = \int \text{Poisson}(N_l|s_l(\theta) + b_l)\, p(b_l|B_l, \delta B_l) db_l, \tag{8}$$

by an exact integration [65] over the expected background b_l. For count experiments that consist of multiple disjoint search regions, we calculate the overall CMS likelihood simply as the

[2] In fact, the expected background count also depends on the SM parameters, but for simplicity we neglect this dependence.

product

$$L(D^{\mathrm{CMS}}|\theta) = \prod_l p(N_l|s_l(\theta)), \tag{9}$$

neglecting the correlation in systematic uncertainties across the search regions.

3.2.4 Likelihood method 2

This method is used for analyses that rely on more complex statistical analysis, based on a likelihood function of the form $L(D^{\mathrm{CMS}}|\mu, \kappa_\theta, \nu)$. Here, D^{CMS} denotes the observed data, κ_θ denotes signal-related parameters for the pMSSM point θ such as signal efficiencies or signal shape parameters for various search regions. With ν we denote nuisance parameters and μ denotes the signal strength, defined as $\mu = \sigma/\sigma(\theta)$, where σ is the unknown actual signal cross section and $\sigma(\theta)$ the predicted signal cross section for pMSSM point θ.

From this input we construct approximate likelihoods that are independent of the nuisance parameters. First we define a test statistic $T_\theta(\mu)$,

$$T_\theta(\mu) = -2\ln\left[\frac{L(D^{\mathrm{CMS}}|\mu, \kappa_\theta, \hat{\hat{\nu}}_\theta(\mu))}{L(D^{\mathrm{CMS}}|\hat{\mu}_\theta, \kappa_\theta, \hat{\nu}_\theta)}\right], \tag{10}$$

where $\hat{\hat{\nu}}_\theta(\mu)$ maximizes $L(D^{\mathrm{CMS}}|\mu, \kappa_\theta, \nu)$ with respect to ν for a particular value of μ and where $\hat{\mu}_\theta$ and $\hat{\nu}_\theta$ maximize $L(D^{\mathrm{CMS}}|\mu, \kappa_\theta, \nu)$ with respect to μ and ν simultaneously. In the asymptotic limit [3], according to Wilks' theorem, $T_\theta(\mu)$ follows a χ^2 distribution with one degree of freedom, under the condition that μ is the true signal strength:

$$p(T_\theta(\mu)|\mu) = \frac{1}{\sqrt{2\pi}}\frac{1}{\sqrt{T_\theta(\mu)}}e^{-T_\theta(\mu)/2}, \tag{11}$$

and thus, we use as CMS likelihood function

$$L(D^{\mathrm{CMS}}|\theta) = p\left(T_\theta(\mu = 1)|\mu = 1\right), \tag{12}$$

with μ set to its predicted value, which is by construction $\mu = 1$. Again, we do not explicitly deal with all signal related uncertainties. Instead, we repeat the calculations with the predicted signal cross section scaled up or down with 50%.

3.3 Calculation of per analysis and combined search sensitivy

A search is sensitive to a certain new physics signal if the analysis can distinguish between the background plus signal hypothesis, denoted here by H_1, and the background-only hypothesis, denoted by H_0. In the current study, the likelihood for hypothesis H_1 at the point θ is given in Eq. (9) or (12), while the likelihood for H_0 is given by the same equations, but with $s_l = 0$ and $\mu = 0$, respectively. For clarity, we use a slightly more precise notation and write the first likelihood, $L(D^{\mathrm{CMS}}|\theta)$, as $L(D^{\mathrm{CMS}}|\theta, H_1)$ and the background-only likelihood as $L(D^{\mathrm{CMS}}|H_0)$.

To determine whether or not a given set of independent CMS data, D^{CMS}, is sensitive to a given pMSSM point θ, we use the score Z defined as

$$Z := \mathrm{sign}(\ln \mathrm{B}_{10})\sqrt{2|\ln \mathrm{B}_{10}|}, \tag{13}$$

[3] And provided that certain conditions are met: mainly, that the likelihood as a function of μ is asymptotically Gaussian.

with B_{10} the *local*[4] Bayes factor,

$$B_{10}(\theta) = L(D^{\text{CMS}}|\theta, H_1)/L(D^{\text{CMS}}|H_0). \tag{14}$$

Since we assume a set of independent data, the overall likelihood function is the product of the likelihood functions for the individual data. The resulting score Z is a signed Bayesian analog of the frequentist "n-sigma". In conventional language, the case $Z \gg 0$ would indicate a signal at "Z-sigma significance", and the case $Z \ll 0$ would indicate a signal *exclusion* at "Z-sigma significance". Note that in our definition of Z, negative values correspond to exclusions while positive values are associated with potential observations, while $Z \sim 0$ corresponds to insensitivity. In particular, for a given pMSSM point θ, $Z < -1.64$. corresponds roughly to a frequentist exclusion at 95% confidence level and a point with $Z > 5$ would signify a discovery.

When dealing with a set of partially overlapping data, we do not define Z as in Eq. (13), since the likelihoods $L(D^{\text{CMS}}|\theta, H_1)$ and $L(D^{\text{CMS}}|H_0)$ in the Bayes factor $B_{10}(\theta)$ cannot be facorized. In such cases we define as large as possible sets of non-overlapping data and in each such set l we obtain a likelihood by multiplying the per datum likelihoods and calculate Z_l with Eq. (13), thereby neglecting correlations between systematic uncertainties of different search regions and between 7 and 8 TeV analyses. Then we define the overall Z value as

$$Z = Z_l, \text{ with } l \equiv \arg\max_j(|Z_j|). \tag{15}$$

Within the considered 7 and 8 TeV analyses, only the 7 TeV HT + MET + b-jets analysis has overlapping search regions. Only for this analysis, we are not able to do a formal combination by taking the product of the likelihoods for each search region. For the remaining 5 analyses, the search regions within each analysis are disjoint. Therefore, for each of these 5 analyses, we are able to do a combination by taking the products of the likelihoods for each search region and present a single combined likelihood for each analysis. The data used for 7 and 8 TeV analyses are disjoint, however the data used by different 7 TeV analyses or different 8 TeV analyses considered in this study are overlapping (e.g. 8 TeV HT + MHT and 8 TeV HT + MET + b-jet analyses are overlapping), therefore we have to use Z values to obtain a combined result for a given center-of-mass energy.

4 Results

In this section we first present the posterior densities for various MSSM masses and the total SUSY production cross section within the context of the pMSSM as defined in Section 2, before and after inclusion of the results of the CMS analyses described in Section 3. We then go on discussing, in subsequent subsections, the current sensitivity of the CMS searches and unexplored regions of parameter space, consequences for the MSSM interpretation of the observed Higgs boson, and finally consequences for neutralino dark matter.

4.1 Posterior densities for parameters, masses and relevant observables

Figure 1 compares prior distributions to posterior distributions including the data from the 7 and 8 TeV HT + MHT searches performed by CMS [57, 60]. Marginalized distributions are shown for several sparticle masses.Blue-gray filled areas depict marginalized non-DCS prior distributions $p^{\text{non-DCS}}(\theta)$, introduced in Section 3.1. Blue line histograms represent marginalized CMS posterior distributions $p(D^{\text{CMS}}|\theta)$, introduced in Section 3.2, for the 7 TeV HT+MHT

[4] *local* as opposed to *global* Bayes factor $B_{10} = L(D^{\text{CMS}}|H_1)/L(D^{\text{CMS}}|H_0)$, in which the likelihood $L(D^{\text{CMS}}|\theta, H_1)$ times the prior $p(\theta|H_1) = p(\theta)$ is marginalized with respect to θ.

data. The red and black line histograms show the similar CMS posterior distributions for respectively the 8 TeV and 7+8 TeV HT+MHT data, where the 7+8 TeV combined posterior probability for each point is obtained by taking a product of the 7 TeV and 8 TeV likelihoods for this search. Solid lines show posterior distributions assuming the central values for the signal cross section, while dashed and dotted lines show posterior distributions assuming respectivel 0.5 and 1.5 times the central values for the signal cross section. The difference between the solid lines and the dotted and dashed lines can be considered as a systematic uncertainty.

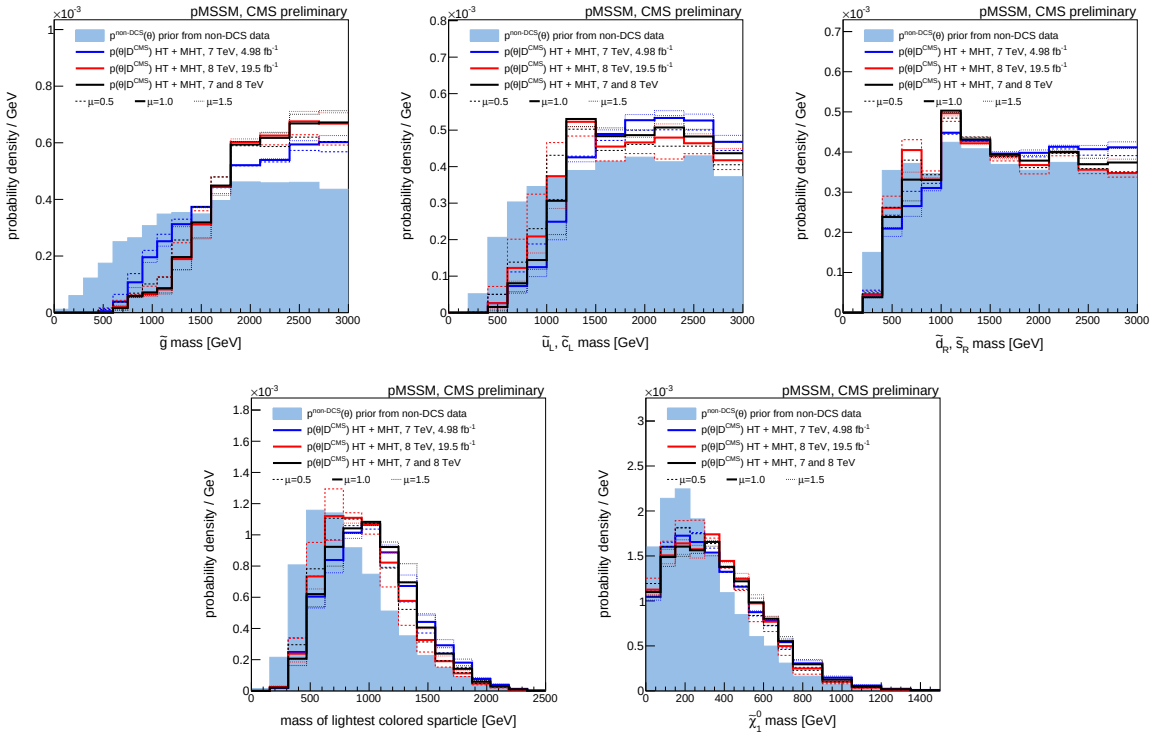

Figure 1: Marginalized distributions of selected sparticle masses. Filled histograms show prior distributions, line histograms show posterior distributions including the data collected at 7 TeV (blue), 8 TeV (red), and 7 and 8 TeV (black) by the CMS HT + MHT searches [57, 60]. The solid curves show posterior densities obtained while assuming the central values for the signal cross section ($\mu = 1$), whereas the dashed and dotted lines show posterior densities obtained with $\pm 50\%$ variations of the signal cross section ($\mu = 0.5$, $\mu = 1.5$).

It appears that the HT+MHT data strongly disfavor pMSSM scenarios with $\tilde{g}$ masses below 1200 GeV. Also scenarios with $\tilde{u}_L, \tilde{c}_L$ masses below 1000 GeV are disfavored. However, the impact on masses of other first and second generation squarks, such as the $\tilde{d}_R, \tilde{s}_R$ masses, is weaker. Regarding third generation squarks, there is a slight impact on the mass of the lightest sbottom, disfavoring the lowest masses, while there is no noticeable impact on the mass of the lightest stop. In more general terms, the most probable mass of the lightest colored sparticle is increased by about 500 GeV. Also the distribution of the $\tilde{\chi}_1^0$ mass is shifted to higher values. This latter effect is mainly a phase space effect, a consequence of our requirement of $\tilde{\chi}_1^0$ to be the LSP: scenarios that are disfavored because of a low gluino or squark mass have necessarily a $\tilde{\chi}_1^0$ that is even lighter.

Figure 2 presents two-dimensional marginalized distributions of the $\tilde{\chi}_1^0$ mass versus the $\tilde{g}$ and $\tilde{u}_L, \tilde{c}_L$ mass, and the ratio of the normalized DCS over non-DCS distributions which display the increase or decrease of probability on the mass plane. This change in probability is of course, as throughout the whole document, calculated assuming that nature is described by

the pMSSM with the parameters within the ranges of Eq 1. These figures clarify how the $\tilde{\chi}_1^0$ mass is shifted to higher values. The aforementioned phase space effect is of course well visible, and in addition a second effect can be observed: for a given squark or gluino mass, regions with low $\tilde{\chi}_1^0$ masses are disfavored more strongly. This feature of the posterior distribution is well known and understood: the higher hadronic activity and higher missing transverse energy of such scenarios make them easier to detect.

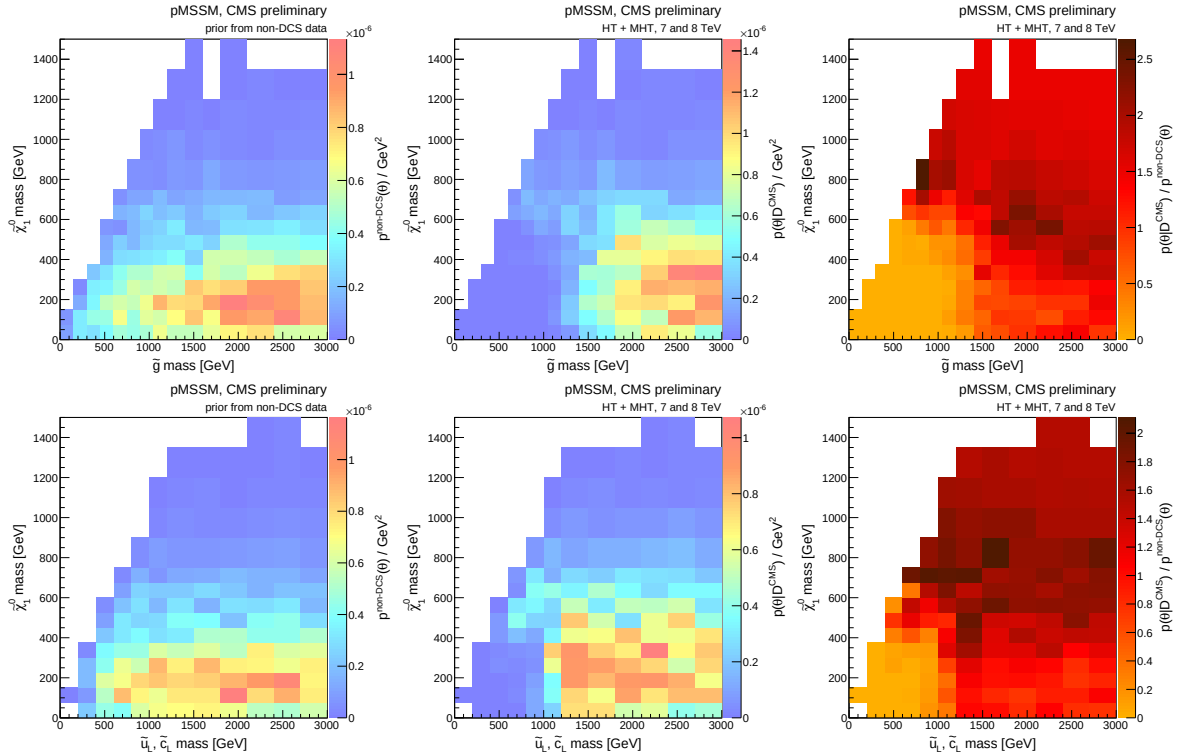

Figure 2: Marginalized 2-dimensional distributions of the $\tilde{\chi}_1^0$ mass versus the $\tilde{g}$ mass (top) and versus the $\tilde{u}_L$ mass (bottom). In each row, the left plot shows the non-DCS prior distribution, the middle plot shows the DCS posterior distribution including the data from the 7 and 8 TeV HT + MHT searches performed by CMS [57, 60], while the plot on the right shows the ratio of the two.

Figure 3 compares prior distributions to posterior distributions for $\tilde{g}$, $\tilde{b}_1$ and $\tilde{t}_1$ masses including the data from the 7 and 8 TeV HT + MET + b-jet searches performed by CMS [58, 61]. In the 7 TeV search, the search regions overlap with each other, and thus we cannot calculate overall 7 TeV or overall 7 and 8 TeV posterior distributions. Instead we calculate posterior distributions for the separate search regions of the 7 TeV search, and show results for the 1b-loose (1BL) region, which requires events to have $\geq$ 1b-jet in addition to loose kinematic requirements. Both the 1BL region of the 7 TeV search and the 8 TeV search disfavor low $\tilde{g}$ masses. The 1BL and 8 TeV data disfavor the lowest $\tilde{b}_1$ masses, whereas the impact of this search on the stop mass is negligible.

Figure 4 compares prior distributions to posterior distributions including the data from the 7 and 8 TeV searches for EW production of charginos, neutralinos and sleptons performed by CMS [59, 62]. The data slightly disfavors the lowest chargino, neutralino and $\tilde{e}_L, \tilde{\mu}_L$ masses. Because this search targets leptons produced in the SUSY cascade, both via off- and on-shell W and Z bosons, it relies on a sizable difference between the mass of the sparticles produced in the hard interaction and the LSP. However, as shown in the top row of Fig. 5, the prior strongly prefers very small mass differences between $\tilde{\chi}_1^0$ and $\tilde{\chi}_1^\pm$ and $\tilde{\chi}_1^0$. Therefore, we introduce the

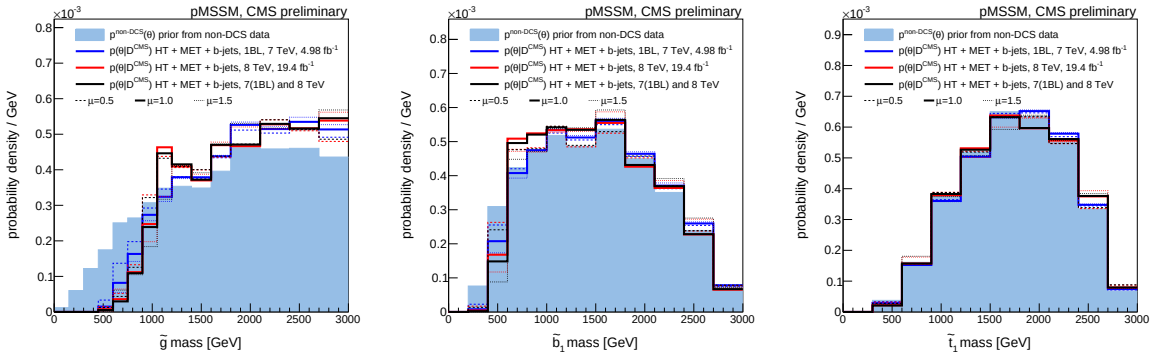

Figure 3: Marginalized distributions of $\tilde{g}$, $\tilde{b}_1$, and $\tilde{t}_1$ mass. Filled histograms show prior distributions, line histograms show posterior distributions including the data collected at 7 TeV (blue), 8 TeV (red), and 7 and 8 TeV (black) by the CMS HT + MET + b-jets searches [58, 61]. The solid curves show posterior densities obtained while assuming the central values for the signal cross section ($\mu = 1$), whereas the dashed and dotted lines show posterior densities obtained with $\pm 50\%$ variations of the signal cross section ($\mu = 0.5$, $\mu = 1.5$). The included 7 TeV data are from the 1BL region of the 7 TeV search.

Lightest Non Degenerate chargino (LND $\tilde{\chi}^{\pm}$) and neutralino (LND $\tilde{\chi}^{0}$) as follows:

$$\text{LND } \chi^{\pm} = \begin{cases} \tilde{\chi}_1^{\pm} & \text{if } |M_1| < \min(|M_2|, |\mu|) \\ \tilde{\chi}_2^{\pm} & \text{if } |M_1| \geq \min(|M_2|, |\mu|) \end{cases} \tag{16}$$

$$\text{LND } \chi^{0} = \begin{cases} \tilde{\chi}_2^{0} & \text{if } |\mu| \geq \min(|M_1|, |M_2|) \\ \tilde{\chi}_3^{0} & \text{if } |\mu| < \min(|M_1|, |M_2|) \end{cases} \tag{17}$$

As shown in the bottom row of Fig. 5, the prior prefers a sizable difference between the mass of these "sparticles" and the LSP, and thus we may expect a larger impact of the 7 and 8 TeV searches for EW production of charginos, neutralinos and sleptons on the LND $\chi^{\pm}$, χ^{0} and χ. Indeed, in Fig. 6 we observe that for LND $\chi^{\pm}$ and χ^{0} the discrepancy between prior and posterior is somewhat larger than for $\tilde{\chi}_1^{\pm}$ and $\tilde{\chi}_2^{0}$ masses.

4.2 Current sensitivity to the pMSSM

In this section we review the overall sensitivity of the considered CMS searches to the pMSSM, and the contributions from the individual searches to this overall sensitivity.

Figure 7 presents distributions of Z, as defined in Section 4.2. Z values are calculated as follows. For both the HT + MHT and the EW analyses, we obtain a 7 TeV, an 8 TeV, and a 7+8 TeV likelihood, making use of Eq. (9), and calculate the corresponding Z values using Eq. (13). For the HT + MET + b-jets analyses, we obtain one 7 TeV likelihood for each of the five statistically dependent 7 TeV signal regions, using Eq. (8), and combine them with Eq. (15). An 8 TeV HT + MET + b-jets likelihood and corresponding Z values are obtained using Eq. (12) and Eq. (13), respectively. We obtain one 7+8 TeV HT + MET + b-jets likelihood for each of the five 7 TeV signal regions by multiplying each 7 TeV likelihood with the 8 TeV likelihood. The corresponding Z values are obtained with Eq. (13) and combined with Eq. (15). Finally, combined 7 TeV Z values are obtained from the aforementioned per analysis 7 TeV Z values with Eq. (15), and combined 8 TeV and combined 7+8 TeV Z values are obtained in the same way.

Each of the distributions peaks near zero, which implies that a large fraction of the pMSSM parameter sub-space under study remains unexplored after having performed the considered

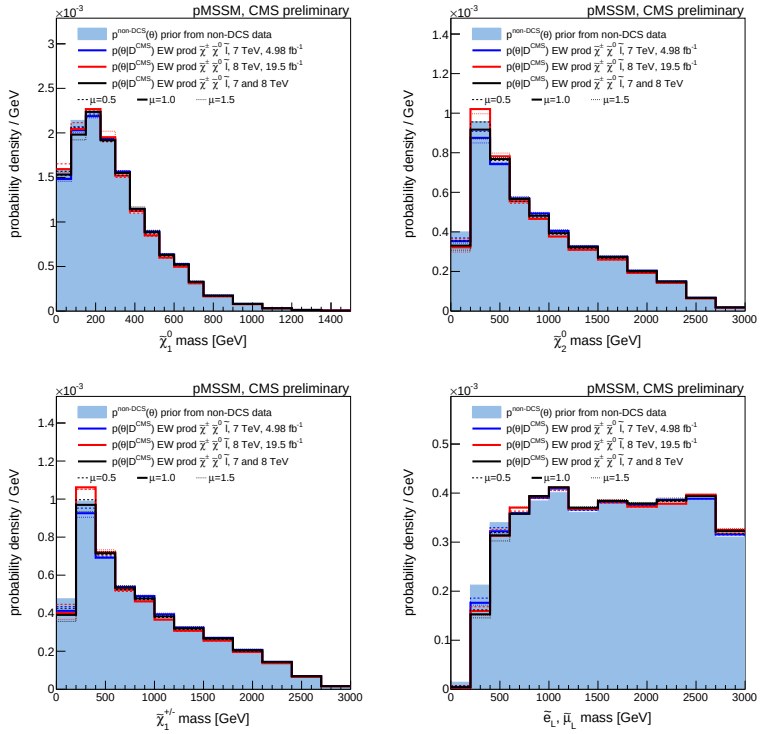

Figure 4: Marginalized distributions of selected sparticle masses. Filled histograms show prior distributions, line histograms show posterior distributions including the data collected at 7 TeV (blue), 8 TeV (red), and 7 and 8 TeV (black) by the CMS searches for EW production of charginos, neutralinos, and sleptons [59, 62]. The solid curves show posterior densities obtained while assuming the central values for the signal cross section ($\mu = 1$), whereas the dashed and dotted lines show posterior densities obtained with $\pm 50\%$ variations of the signal cross section ($\mu = 0.5$, $\mu = 1.5$).

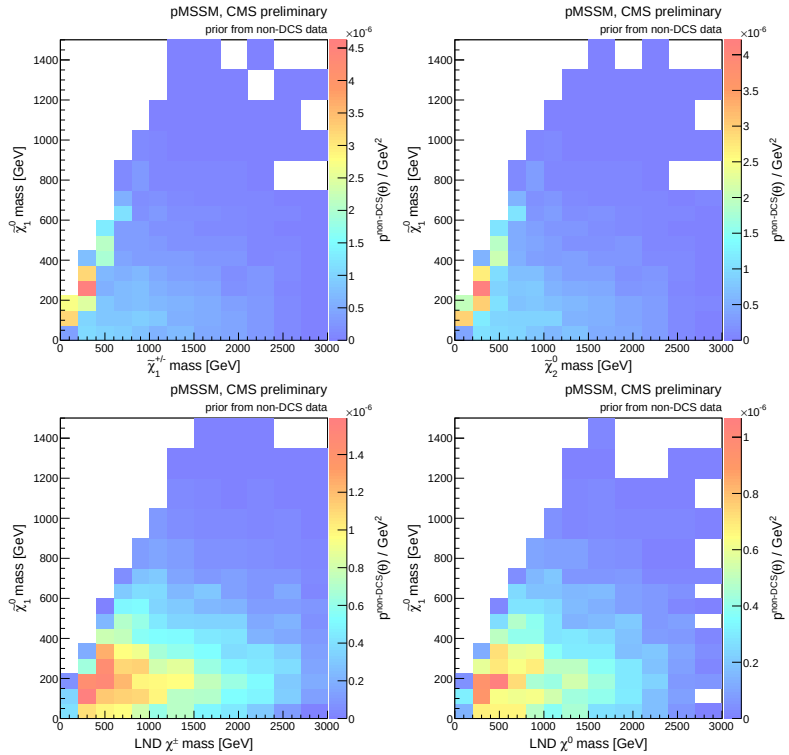

Figure 5: Marginalized 2-dimensional prior distributions of the $\tilde{\chi}_1^0$ mass versus the $\tilde{\chi}_1^{\pm}$ mass (top-left), versus the $\tilde{\chi}_2^0$ mass (top-right), versus the Lightest Non Degenerate (LND) $\chi^{\pm}$ mass (bottom-left), and versus the LND χ^0 mass (bottom-right).

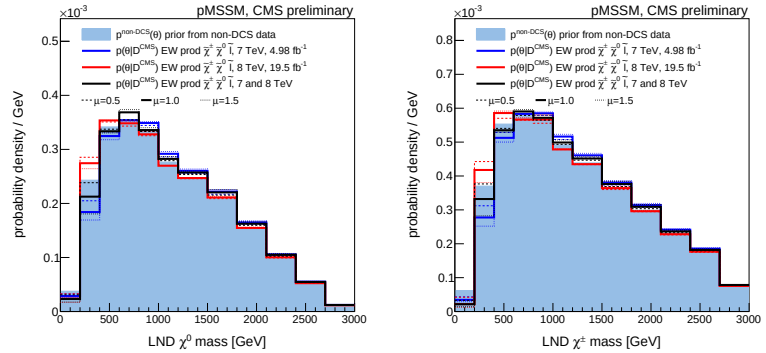

Figure 6: Marginalized distributions of the masses of Lightest Non Degenerate (LND) $\chi^{\pm}$ and χ^0. Filled histograms show prior distributions, line histograms show posterior distributions including the data collected at 7 TeV (blue), 8 TeV (red), and 7 and 8 TeV (black) by the CMS searches for EW production of charginos, neutralinos, and sleptons [59, 62]. The solid curves show posterior densities obtained while assuming the central values for the signal cross section ($\mu = 1$), whereas the dashed and dotted lines show posterior densities obtained with $\pm 50\%$ variations of the signal cross section ($\mu = 0.5$, $\mu = 1.5$).

CMS searches. The left tail of these distributions corresponds to the fraction of the pMSSM parameter space that is in disagreement with the CMS data. This tail is especially pronounced for the two hadronic searches. On the right side of the peaks, where data would prefer particular signal scenarios, we observe rarely Z values above 3.

Table 3 shows the probabilities $p(Z < -1.64)$, $p(Z < -3)$, $p(Z < -5)$ per search and per dataset, in other words, fractions of parameter space with respectively a Z value below -1.64, below -3, and below -5. Between brackets we show the corresponding fraction of phases space for which the particlar analysis is the one and only analysis with Z value below the respective threshold value.

Table 3: Probabilities $p(Z < -1.64)$, $p(Z < -3)$, $p(Z < -5)$ per search and per dataset, in other words, fractions of phase space with respective Z values below -1.64, -3, and -5. Between brackets we show the corresponding fraction of parameter space for which the particlar analysis is the one and only analysis with Z value below the respective threshold value.

	$p(Z < -1.64)$		$p(Z < -3)$		$p(Z < -5)$	
	7 TeV					
HT + MHT	0.40	(0.23)	0.26	(0.15)	0.17	(0.09)
HT + MET + b-jets	0.19	(0.02)	0.14	(0.02)	0.098	(0.02)
EW prod. $\tilde{\chi}^{\pm}, \tilde{\chi}^{0}, \tilde{l}$	0.026	(0.008)	0.011	(0.005)	0.005	(0.002)
combination	0.42		0.29		0.19	
	8 TeV					
HT + MHT	0.45	(0.16)	0.37	(0.16)	0.30	(0.14)
HT + MET + b-jets	0.31	(0.03)	0.23	(0.02)	0.17	(0.02)
EW prod. $\tilde{\chi}^{\pm}, \tilde{\chi}^{0}, \tilde{l}$	0.050	(0.019)	0.029	(0.013)	0.016	(0.008)
combination	0.47		0.41		0.32	
	7 and 8 TeV					
HT + MHT	0.48	(0.16)	0.40	(0.16)	0.32	(0.14)
HT + MET + b-jets	0.34	(0.03)	0.26	(0.02)	0.19	(0.02)
EW prod. $\tilde{\chi}^{\pm}, \tilde{\chi}^{0}, \tilde{l}$	0.055	(0.017)	0.032	(0.012)	0.018	(0.007)
combination	0.51		0.44		0.34	

We construct posterior distributions including the data from all CMS searches under consideration, using a binary likelihood as the CMS likelihood

$$L(D^{\text{CMS}}|\theta) = \begin{cases} 0 & \text{if } Z < -1.64 \\ 1 & \text{if } Z \geq -1.64 \end{cases} \tag{18}$$

where Z was calculated for the combined data from all considered searches. Figure 8 compares prior distributions to posterior distributions constructed with this likelihood. Note that the distribution of the cross section is particularly dependent on the volume of our pMSSM subspace. Extending the mass parameters to higher values would increase the likelihood in the low cross section values.

An alternative way to present the sensitivity of CMS to the pMSSM makes use of the *survival probability*. We define the survival probability p_{Θ}^{surv} in a certain region Θ of the pMSSM parameter space as

$$p_{\Theta}^{\text{surv}} = \frac{\int_{\Theta} H\left(Z(\theta) + 1.64\right) p^{\text{non-DCS}}(\theta) d\theta}{\int_{\Theta} p^{\text{non-DCS}}(\theta) d\theta}, \tag{19}$$

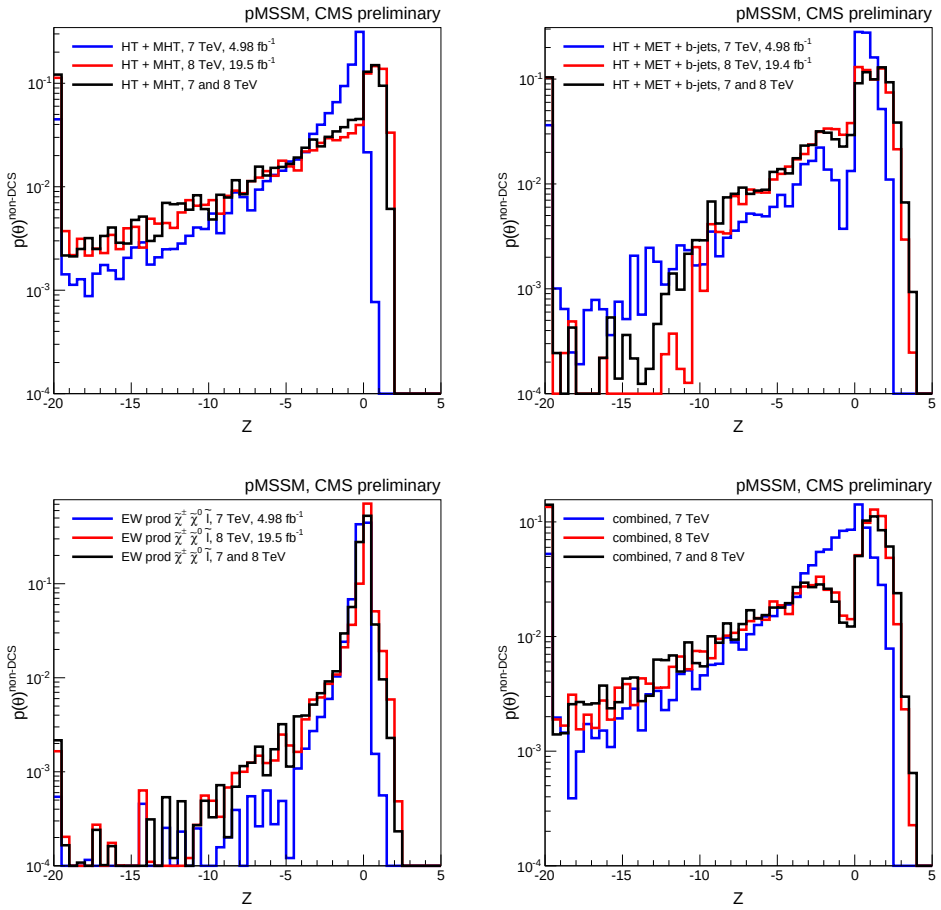

Figure 7: Distributions of Z for the CMS HT + MHT searches (top-left), the CMS HT + MET + b-jets searches (top-right), the CMS searches for EW production of charginos, neutralinos, and sleptons (bottom-left), and their combinations (bottom-right). Blue, red, and black line histograms show Z distributions including the data collected at respectively 7 TeV, 8 TeV, and 7 and 8 TeV. In each distribution, the first and last bin show respectively the under and overflow of the histogram.

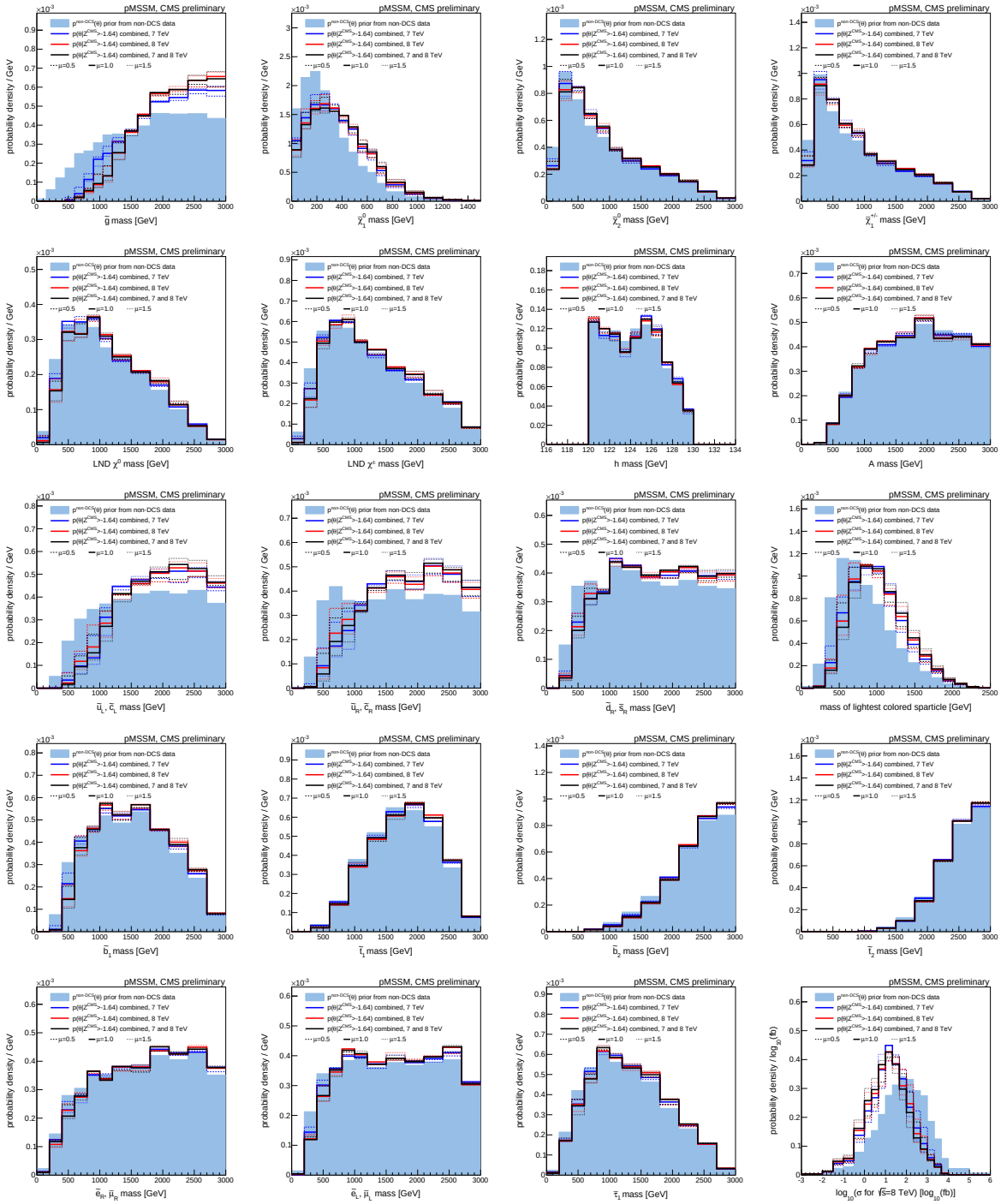

Figure 8: Marginalized distributions of selected sparticle masses and total sparticle production cross section. Filled histograms show prior distributions, line histograms show posterior distributions including the data collected at 7 TeV (blue), 8 TeV (red), and 7 and 8 TeV (black) by the CMS searches [57–62]. The solid curves show posterior densities obtained while assuming the central values for the signal cross section ($\mu = 1$), whereas the dashed and dotted lines show posterior densities obtained with $\pm 50\%$ variations of the signal cross section ($\mu = 0.5$, $\mu = 1.5$). Note that the distribution of the $\log_{10}$ of the cross section is particularly dependent on the volume of our pMSSM subspace.

where H is the Heaviside step function. In our discrete representation this becomes

$$p_{\Theta}^{\text{surv}} = \frac{\sum_{\theta\in\Theta} w_\theta H\left(Z(\theta)+1.64\right)}{\sum_{\theta\in\Theta} w_\theta} \tag{20}$$

with w_θ the weight of pMSSM point θ used to introduce non-DCS data in the chain of inference after pMSSM points were sampled with the MCMC. Figure 9 shows the survival probability for selected sparticle masses and for the total sparticle production cross section for 7 TeV, 8 TeV and $7+8$ TeV.

As we can see, the survival probability for the colored sparticles is significantly lower for the low masses. However, scenarios with very light colored sparticles can still survive the CMS searches. We have investigated the characteristics of several such cases. One regular case is that for light gluinos and stops, the gluino or stop is the next-to-lightest superparticle and is nearly degenerate with a $\tilde{\chi}_1^0$ that weighs a few hundred GeV . In such cases there is relatively little visible activity, making it difficult to distinguish signal events from background events. Another well-known case is the presence of multiple near-degenerate EW gauginos between the gluino or the stop and the $\tilde{\chi}_1^0$. This case is defined as a compressed spectrum, and leads to multiple soft decay products, which are hard to discriminate with the current data.

4.3 Consequences for the Higgs boson sector

In this section, we investigate the possible impact of the CMS SUSY searches on the Higgs sector of the MSSM. To this end, we employ a tighter selection of 123 GeV $\leq m_h \leq$ 128 GeV in order to comply with the measured Higgs boson mass of about 125.5 GeV, including the 2–3 GeV theoretical uncertainty in the calculation of the light Higgs boson mass in the MSSM. Note that this tighter m_h window is relevant *only* for discussing the 125 GeV Higgs boson signal, and is thus applied *only* in this section. Indeed, once the non-DCS constraints are imposed, the only SUSY parameters which are significantly affected by an additional requirement on m_h are A_t and the stop mixing parameter X_t/M_{SUSY}, with the usual definitions $X_t \equiv A_t - (\mu/\tan\beta)$ and $M_{\text{SUSY}} = \sqrt{m_{\tilde{t}_1} m_{\tilde{t}_2}}$. This is discussed in some detail in Ref. [66].

It is well known that to achieve $m_h \approx 125$ GeV either the stops must be very heavy, or $|A_t|$ and $|X_t/M_{\text{SUSY}}|$ must be large, only slightly shy of the so-called maximal mixing choice $|X_t/M_{\text{SUSY}}| \sim \sqrt{6}$ (see [66] and references therein). However, once 123 GeV $\leq m_h \leq$ 128 GeV is required, the CMS SUSY data have little impact on either this ratio or $m_{\tilde{t}_1}$. This is illustrated in Fig. 10, which shows the non-DCS probability distribution, the DCS posterior density as well as the ratio of the two in the X_t/M_{SUSY} versus $m_{\tilde{t}_1}$ plane. From the left plot, we see that the bulk of the points have $m_{\tilde{t}_1} > 1$ TeV and a large stop mixing parameter of $X_t/M_{\text{SUSY}} \sim 1.5$ or ~ -2. The middle and right-hand plots illustrate the fact that the CMS data cause only a slight shift of the $\tilde{t}_1$ mass posterior distribution to higher values.

One way to test the orthogonality [34, 66] of the Higgs boson measurements and SUSY exclusions is to consider the impact of the latter on the production/decay rates for the SM-like Higgs boson itself. In other words, how do the predicted signal strengths compare to the measured ones, and do the CMS SUSY searches have any impact on them? To answer such questions we define Higgs boson signal strengths $\mu_X(Y)$ for given initial states X and final states Y:

$$\mu_X(Y) = \frac{\sigma(X\to h)\text{BR}(h\to Y)}{\sigma_{\text{SM}}(X\to h_{\text{SM}})\text{BR}(h_{\text{SM}}\to Y)}. \tag{21}$$

The production processes of interest are gluon fusion, $X = gg$, vector-boson fusion, $WW, ZZ \to h$, commonly denoted by $X = VBF$, and vector boson plus Higgs boson associated production,

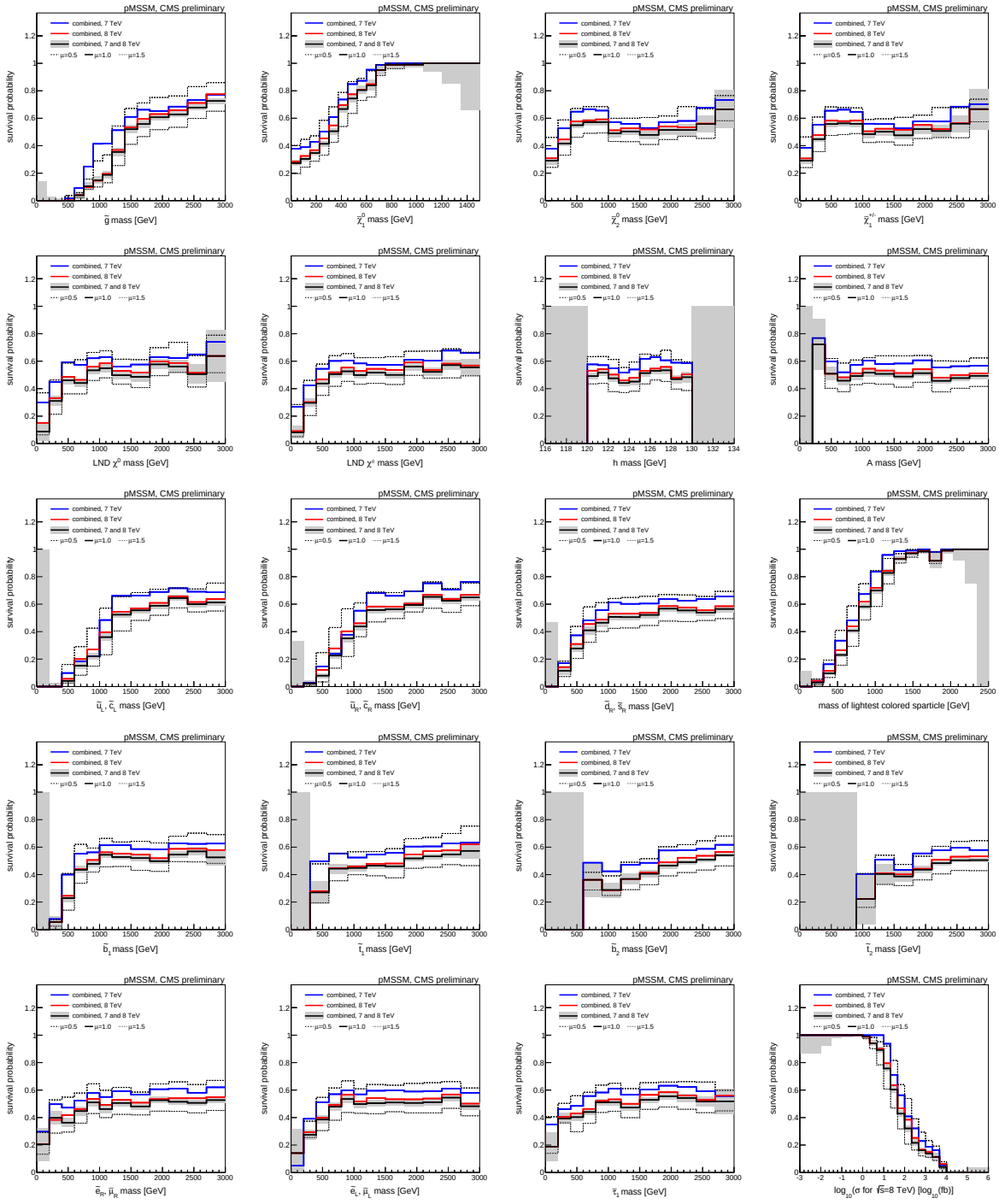

Figure 9: Survival probabilities as a function of selected sparticle masses and total sparticle production cross section, after the data from the searches performed by CMS [57–62]. Line histograms show survival probabilities after 7 TeV (blue), 8 TeV (red), and 7 and 8 TeV (black) data. The solid curves show survival probabilities obtained while assuming the central values for the signal cross section ($\mu = 1$), whereas the dashed and dotted lines show survival probabilities obtained with $\pm 50\%$ variations of the signal cross section ($\mu = 0.5$, $\mu = 1.5$). The filled area represents the statistical uncertainty.

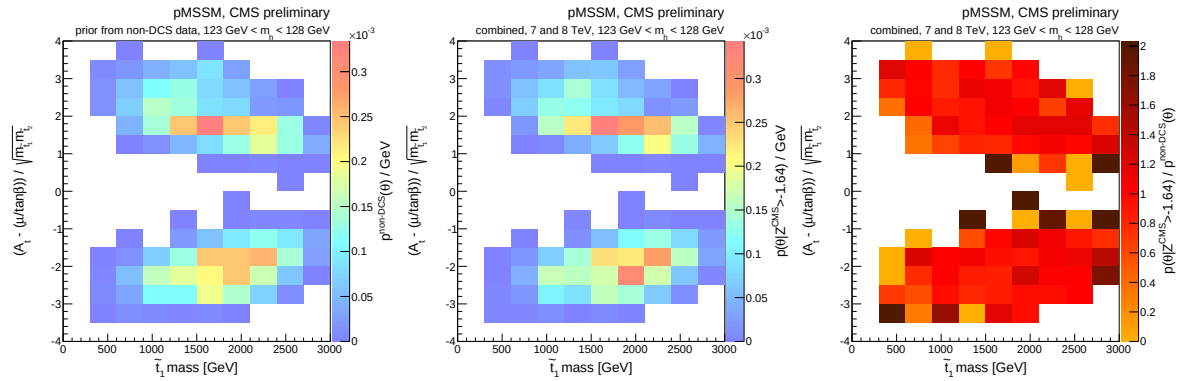

Figure 10: Marginalized 2-dimensional distributions of $X_t/M_{\rm SUSY}$ vs. $m_{\tilde{t}_1}$. The left plot shows the non-DCS prior distribution, the middle plot shows the DCS posterior distribution including the data from the 7 and 8 TeV searches performed by CMS [57–62], while the plot on the right shows the ratio of the two. In all plots 123 GeV $\leq m_h \leq$ 128 GeV is required.

denoted by $X = Vh$. In two-doublet models such as the MSSM the scale factor for $X = Vh$ is the same as for $X = VBF$ [67] and so we only show the latter. The final states of interest are $Y = \gamma\gamma$, ZZ, WW, $\tau\tau$, and bb. In any two-doublet model, the scale factor for $Y = WW$ is the same as that for $Y = ZZ$ [67], so again we only plot the latter. Similarly, to first approximation the $\tau\tau$ scale factor is the same as that for bb.

In the upper row of Fig. 11, we present probability densities for $\mu_{gg}(\gamma\gamma)$, $\mu_{gg}(ZZ)$, and $\mu_{gg}(bb)$. The corresponding results for the VBF initial state are given in the lower row of Fig. 11. Imposing $Z > -1.64$ in addition to the non-DCS requirements has a rather modest impact in these and all subsequent plots in this section. Thus, most remarks in this section can be taken to apply to both the non-DCS and $Z > -1.64$ distributions.

Returning to the $\mu_X(Y)$ ratios, we observe a strong peaking at values near 1, but ranging with significant probability to values as large as $1.2 - 1.4$ in the $\gamma\gamma$ and ZZ final states, with the bb final state tending to have $\mu_{gg}(bb)$ values more tightly clustered near unity. The fact that the $\mu_X(Y)$ distributions tend to peak at values close to 1 already at the non-DCS level implies that the light h is most likely quite SM-like, despite the very large range of MSSM parameter choices being sampled. In fact, current measurements of the Higgs boson $\mu_X(Y)$ ratios are completely consistent with SM-like values of unity, as shown in Fig. 4 of [66], and narrow the $\mu_X(Y)$ distributions substantially relative to the non-DCS distributions shown. In contrast, we find that the $\mu_X(Y)$ distributions are not much impacted by CMS data regarding searches for SUSY. In other words, the SUSY limits are 'orthogonal' to the direct Higgs boson measurements.

Of course, it would be extremely exciting if one of the other Higgs bosons of the MSSM, H, A or $H^\pm$, could be detected. First, we note that the decoupling result of $m_H \sim m_A \sim m_{H^\pm}$ sets in already for $m_A \sim 500$ GeV. Further, one finds that the lowest value of m_A with significant non-DCS posterior probability is of order 500 GeV with $m_A \geq 800$ GeV having greater than 95% probability. Indeed, there is significant probability extending all the way up to 3 TeV and higher. To get an idea of the impact of CMS SUSY data, in Fig. 12 we present probability densities in the $\tan\beta$ vs. m_A plane requiring 123 GeV $< m_h <$ 128 GeV. The left plot shows the non-DCS probability distribution, the middle plot gives the DCS posterior density for $Z > -1.64$ while the right plot displays the ratio of the two. Note that the $7 + 8$ TeV data narrow the most probable wedge region somewhat in the direction of lower $\tan\beta$ at any given m_A. Comparing the latter to current limits [68, 69] obtained assuming $m_H \sim m_A$ and neglecting interference (both approximations being adequate given the limited mass resolution in the $\tau\tau$

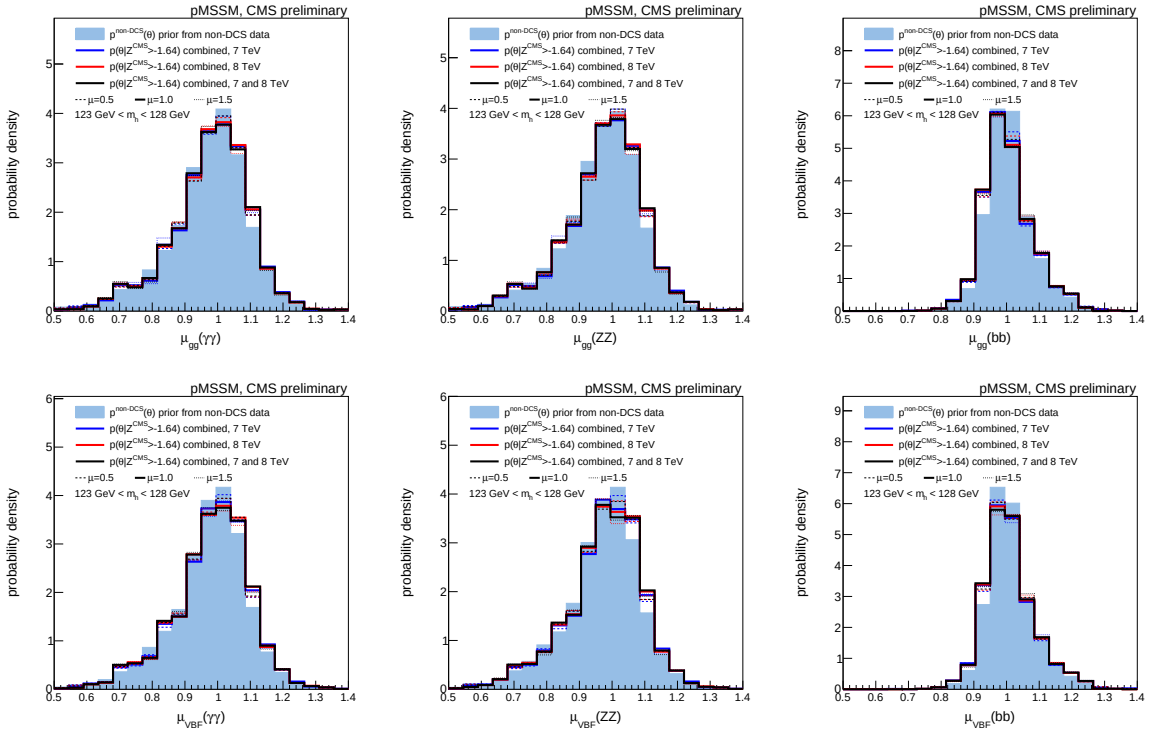

Figure 11: Marginalized distributions of $\mu_{gg}(\gamma\gamma)$, $\mu_{gg}(ZZ)$, and $\mu_{gg}(bb)$ (upper row) and for $\mu_{VBF}(\gamma\gamma)$, $\mu_{VBF}(ZZ)$, and $\mu_{VBF}(bb)$ (lower row). Filled histograms show prior distributions, line histograms show posterior distributions including the data collected at 7 TeV (blue), 8 TeV (red), and 7 and 8 TeV (black) by the CMS searches [57–62]. The solid curves show posterior densities obtained while assuming the central values for the signal cross section ($\mu = 1$), whereas the dashed and dotted lines show posterior densities obtained with $\pm 50\%$ variations of the signal cross section ($\mu = 0.5$, $\mu = 1.5$). In all plots 123 GeV $\leq m_h \leq$ 128 GeV is required.

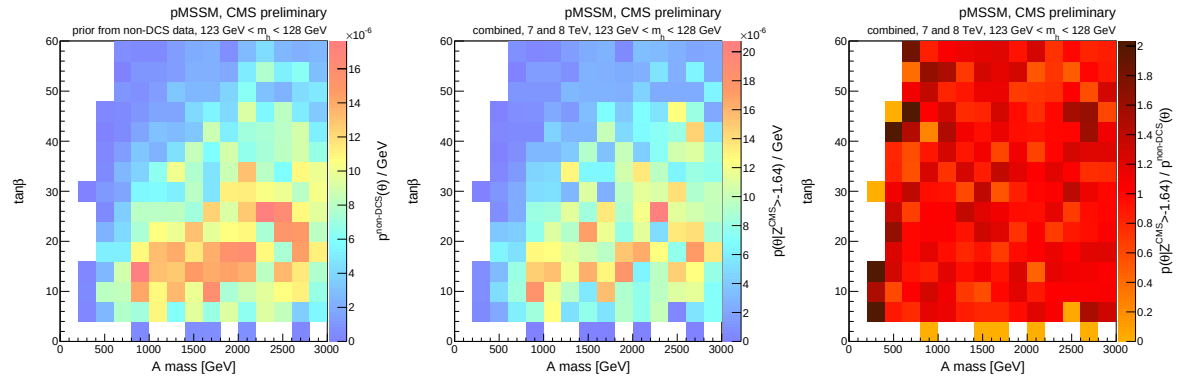

Figure 12: Marginalized 2-dimensional distributions of $\tan\beta$ vs. m_A. The left plot shows the non-DCS prior distribution, the middle plot shows the DCS posterior distribution including the data from the 7 and 8 TeV searches performed by CMS [57–62], while the plot on the right shows the ratio of the two. In all three plots 123 GeV $\leq m_h \leq$ 128 GeV is required.

final state), we find that most points in this plane are allowed. Only a few low probability points at very high $\tan\beta$ values at a given m_A would be excluded. The fact that the allowed wedge is close to the current limits from the $\tau^+\tau^-$ mode implies that the next LHC run could observe the A, H if $\tan\beta$ is near the upper limit allowed by the current data set. It should be noted that the Higgs boson precision measurements actually constrain the wedge more strongly than either non-DCS data or CMS SUSY searches, as shown in the upper-right plot of Fig. 6 of [66].

Finally, it is interesting to assess the extent to which the $H, A, H^\pm$ might be observable via decays into supersymmetric final states. For most of the non-DCS preferred parameter space, such decays have very small branching ratio. The $Z > -1.64$ requirement after including CMS data results in a small shift to still lower SUSY branching ratios. However, for a small, but significant fraction of the parameter space these Higgs bosons decay with a substantial branching ratio (reaching as high as 90%) to superpartner-pair final states. These superpartner-pair final states are typically not pairs of LSPs but sparticles that give potentially visible signatures — the branching ratios for decay to the invisible $\tilde{\chi}_1^0\tilde{\chi}_1^0$ final state are always very small, even when kinematically allowed.

4.4 Consequences for Dark Matter

Although we assume R-parity conservation and a neutralino LSP, we chose not to apply any dark matter (DM) constraints on the neutralino in the sampling of the pMSSM parameter space. This is to avoid making assumptions about the history of the Universe (such as pure thermal production of particles, only one DM candidate, constant entropy after freeze-out, etc.) as usually enter the "vanilla" DM constraints. Instead, in this section we test the influence of the CMS SUSY searches on DM-related quantities, such as the would-be neutralino relic density, $\Omega_{\tilde{\chi}_1^0}h^2$ (assuming standard cosmology) and the expected spin-dependent (SD) and spin-independent (SI) cross sections for scattering off protons, which are relevant for direct DM searches.

The marginalized 1D posterior density distributions of $\Omega_{\tilde{\chi}_1^0}h^2$, $\xi\sigma^{\mathrm{SD}}$, and $\xi\sigma^{\mathrm{SI}}$ are shown in Fig. 13. The rescaling factor $\xi \equiv \Omega_{\tilde{\chi}_1^0}h^2/0.119$ is applied to normalize the $\tilde{\chi}_1^0 p$ scattering cross section to the DM relic density $\Omega h^2 \simeq 0.119$ determined by PLANCK [70]; this is useful because the limits set by the direct DM detection experiments assume that only one type of particles makes up all the DM.

We note first of all a two-peak structure in the distribution of $\Omega_{\tilde{\chi}_1^0}h^2$, with the minimum actually lying near the cosmologically preferred value of $\approx$ 0.1. With an estimated 10% theoretical

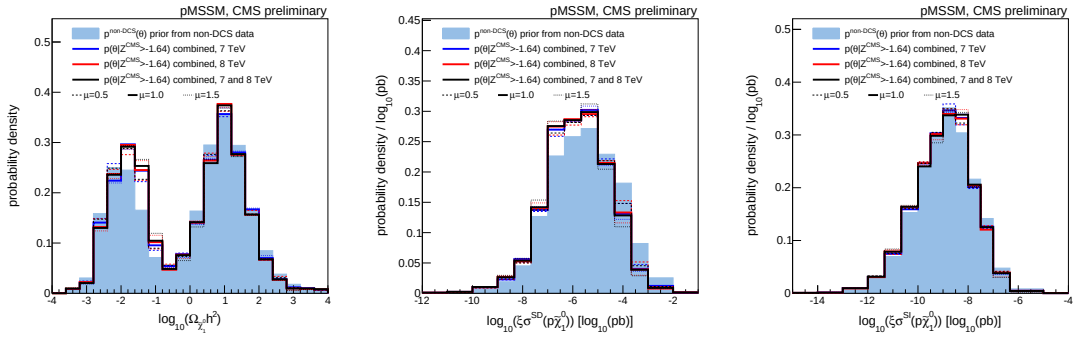

Figure 13: Marginalized distributions of neutralino relic density $\Omega_{\tilde{\chi}_1^0}h^2$ (left), spin-dependent direct dark matter (DM) detection cross section $\xi\sigma^{\mathrm{SD}}$ (middle), and spin-independent direct DM detection cross section $\xi\sigma^{\mathrm{SI}}$ (right), with the rescaling factor $\xi = \Omega_{\tilde{\chi}_1^0}h^2/0.119$. Filled histograms show prior distributions, line histograms show posterior distributions including the data collected at 7 TeV (blue), 8 TeV (red), and 7 and 8 TeV (black) by the CMS searches [57–62]. The solid curves show posterior densities obtained while assuming the central values for the signal cross section ($\mu = 1$), whereas the dashed and dotted lines show posterior densities obtained with $\pm 50\%$ variations of the signal cross section ($\mu = 0.5$, $\mu = 1.5$).

uncertainty on the measured DM relic density, the probability at the non-DCS level to have a relic density that is too high (too low) is about 63.3% (36.3%), while the probability of being within 10% of the PLANCK value is $p(0.107 \leq \Omega_{\tilde{\chi}_1^0}h^2 \leq 0.131) \approx 0.5\%$. The effect of the CMS searches is to slightly shift the $\Omega_{\tilde{\chi}_1^0}h^2$ distribution towards lower values, but the two-peak structure and the minimum around $\Omega_{\tilde{\chi}_1^0}h^2 \sim 0.1$ remain; there is however a very slight increase to $p(0.107 \leq \Omega_{\tilde{\chi}_1^0}h^2 \leq 0.131) \sim 0.6\%$ for $Z > -1.64$. The corresponding scattering cross sections off protons are however challenged by the limits from direct DM searches; in particular LUX excludes $\xi\sigma^{\mathrm{SI}}(\tilde{\chi}_1^0 p) \gtrsim 10^{-9}-10^{-8}$ pb for DM masses of 100 – 1000 GeV (at 90% CL) [71].

The possible complementarity between collider and astrophysics experiments for pinning down the nature of DM (and eventually testing the standard cosmological model) becomes somewhat more apparent in the 2D distributions of $\Omega_{\tilde{\chi}_1^0}h^2$ and $\xi\sigma(\tilde{\chi}_1^0 p)$ versus $\tilde{\chi}_1^0$ mass, shown in Fig. 14. While the influence of current CMS results at 7 and 8 TeV is still marginal, it becomes clear that the CMS searches are beginning to test the most interesting region with LSP masses below about 400–500 GeV. Finally, note that the plots of this section can be compared to Figs. 10 and 11 of [66], which show the influence of the Higgs signal strength likelihood on the distributions of $\Omega_{\tilde{\chi}_1^0}h^2$ and $\xi\sigma^{\mathrm{SI}}(\tilde{\chi}_1^0 p)$.

5 Conclusions

We have investigated the impact of a subset of the 7 and 8 TeV CMS SUSY searches on a potentially accessible sub-space of the pMSSM, a 19-dimensional proxy of the MSSM defined at the SUSY scale. The sub-space is sampled using an MCMC method that covers sparticle masses up to about 3 TeV. The analyses span a variety of final states, which permit a broad exploration of the pMSSM, and by association the MSSM. We only consider the phase space where the chargino lifetime $c\tau(\tilde{\chi}_1^{\pm})$ is less than 10 mm.

We have interpreted the results from HT + MHT, HT + MET + b-jets, and leptonic EW searches. We have also calculated the effect of the combination of the 7 and 8 TeV CMS SUSY results.

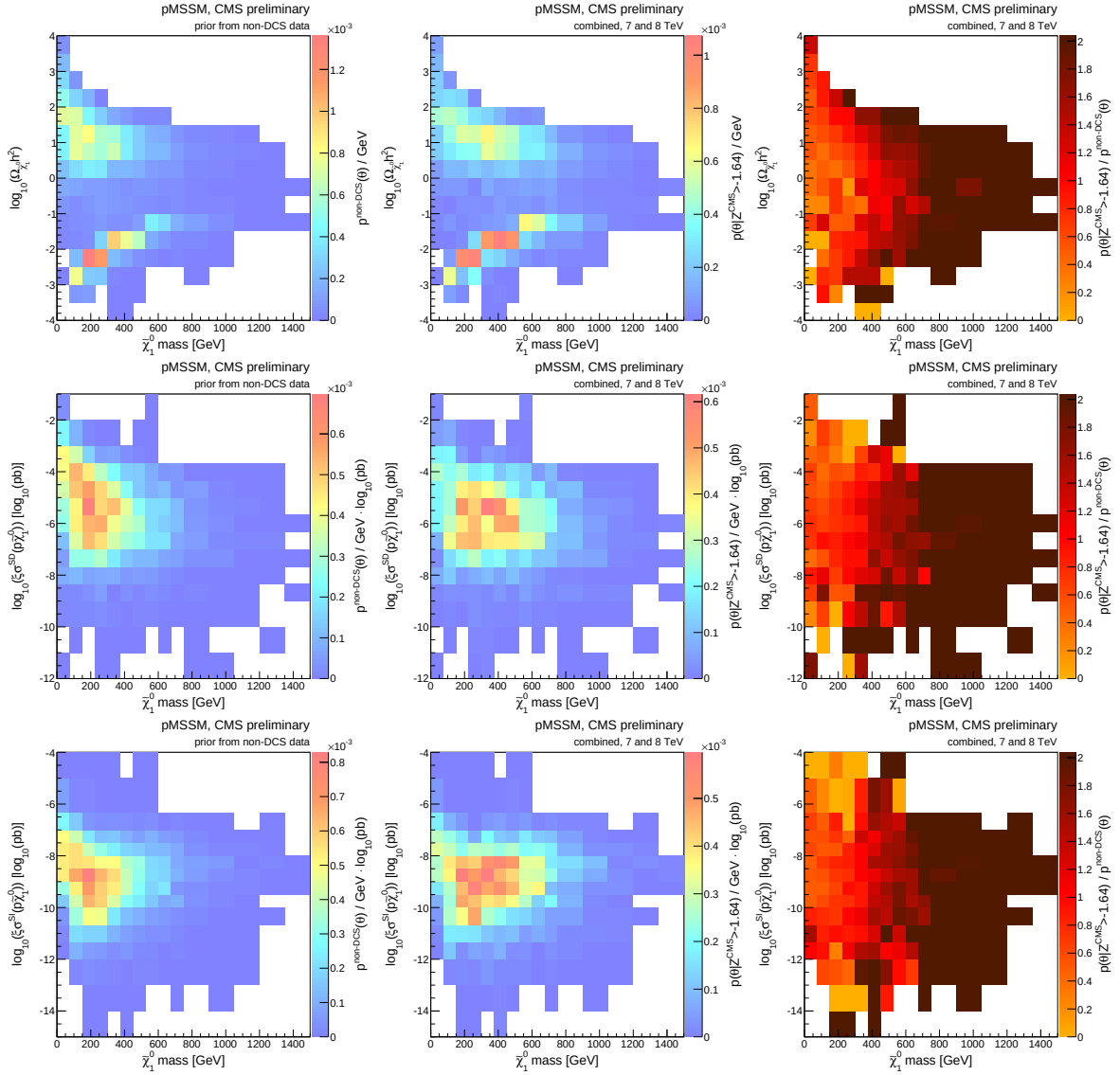

Figure 14: Marginalized 2-dimensional distributions of neutralino relic density $\Omega_{\tilde{\chi}_1^0}h^2$ (top row), spin-dependent direct dark matter (DM) detection cross section $\xi\sigma^{SD}$ (middle row), and spin-independent direct DM detection cross section $\xi\sigma^{SI}$ (bottom row), versus $\tilde{\chi}_1^0$ mass with the rescaling factor $\xi = \Omega_{\tilde{\chi}_1^0}h^2/0.119$. In each row, the left plot shows the non-DCS prior distribution, the middle plot shows the DCS posterior distribution including the data from the 7 and 8 TeV searches performed by CMS [57–62], while the plot on the right shows the ratio of the two.

We have considered 50% variations on the pMSSM signals to take into account signal related systematic uncertainties, while we have neglected the correlations between background predictions for different search regions and for the 7 and 8 TeV data sets. Our overall conclusion is that the hadronic 7 and 8 TeV CMS analyses have a significant impact on the allowed values of the gluino and light-flavor squark masses, but third-generation squarks are much less affected. In particular, there is no visible effect of the considered hadronic inclusive searches on the stop mass distributions. We also see a slight limiting of the $\widetilde{\chi}_1^0$ mass distribution, which is an indirect constraint arising from the fact that $\widetilde{\chi}_1^0$ is the LSP. The leptonic EW analyses on the other hand have only a slight effect on neutralino, chargino and slepton masses. This study demonstrates that a rigorous approach to testing the general MSSM, without theoretical prejudices on the patterns of SUSY soft-breaking terms, is absolutely feasible.

References

[1] ATLAS Collaboration, "Observation of a new particle in the search for the Standard Model Higgs boson with the ATLAS detector at the LHC", *Phys.Lett.* **B716** (2012) 1–29, doi:10.1016/j.physletb.2012.08.020, arXiv:1207.7214.

[2] CMS Collaboration, "Observation of a new boson at a mass of 125 GeV with the CMS experiment at the LHC", *Phys.Lett.* **B716** (2012) 30–61, doi:10.1016/j.physletb.2012.08.021, arXiv:1207.7235.

[3] S. P. Martin, "A Supersymmetry Primer", arXiv:hep-ph/9709356.

[4] D. Chung et al., "The soft supersymmetry breaking Lagrangian: Theory and applications", *Phys.Rept.* **407** (2005) 1–203, doi:10.1016/j.physrep.2004.08.032, arXiv:hep-ph/0312378.

[5] A. H. Chamseddine, R. L. Arnowitt, and P. Nath, "Locally Supersymmetric Grand Unification", *Phys.Rev.Lett.* **49** (1982) 970, doi:10.1103/PhysRevLett.49.970.

[6] R. Barbieri, S. Ferrara, and C. A. Savoy, "Gauge Models with Spontaneously Broken Local Supersymmetry", *Phys.Lett.* **B119** (1982) 343, doi:10.1016/0370-2693(82)90685-2.

[7] L. E. Ibanez, "Locally Supersymmetric SU(5) Grand Unification", *Phys.Lett.* **B118** (1982) 73, doi:10.1016/0370-2693(82)90604-9.

[8] L. J. Hall, J. D. Lykken, and S. Weinberg, "Supergravity as the Messenger of Supersymmetry Breaking", *Phys.Rev.* **D27** (1983) 2359–2378, doi:10.1103/PhysRevD.27.2359.

[9] P. Nath, "Twenty years of SUGRA", arxiv preprint, 2003.

[10] G. L. Kane, C. F. Kolda, L. Roszkowski, and J. D. Wells, "Study of constrained minimal supersymmetry", *Phys.Rev.* **D49** (1994) 6173–6210, doi:10.1103/PhysRevD.49.6173, arXiv:hep-ph/9312272.

[11] H. Baer et al., "Multichannel search for minimal supergravity at $p\bar{p}$ and e^+e^- colliders", *Phys.Rev.* **D51** (1995) 1046–1050, doi:10.1103/PhysRevD.51.1046, arXiv:hep-ph/9408265.

[12] J. Alwall, P. Schuster, and N. Toro, "Simplified Models for a First Characterization of New Physics at the LHC", *Phys.Rev.* **D79** (2009) 075020, doi:10.1103/PhysRevD.79.075020, arXiv:0810.3921.

[13] LHC New Physics Working Group, "Simplified Models for LHC New Physics Searches", *J.Phys.* **G39** (2012) 105005, doi:10.1088/0954-3899/39/10/105005, arXiv:1105.2838.

[14] CMS Collaboration, "Interpretation of Searches for Supersymmetry with simplified Models", *Phys.Rev.* **D88** (2013) 052017, doi:10.1103/PhysRevD.88.052017, arXiv:1301.2175.

[15] MSSM Working Group, "The Minimal supersymmetric standard model: Group summary report", arXiv:hep-ph/9901246.

[16] CMS Collaboration, "Phenomenological MSSM interpretation of the CMS 2011 5fb^{-1} result", cms physics analysis summary, 2012.

[17] S. Sekmen et al., "Interpreting LHC SUSY searches in the phenomenological MSSM", *JHEP* **1202** (2012) 075, doi:10.1007/JHEP02(2012)075, arXiv:1109.5119.

[18] CMS Collaboration, "Search for Supersymmetry at the LHC in Events with Jets and Missing Transverse Energy", *Phys.Rev.Lett.* **107** (2011) 221804, doi:10.1103/PhysRevLett.107.221804, arXiv:1109.2352.

[19] CMS Collaboration, "Search for new physics with same-sign isolated dilepton events with jets and missing energy", cms physics analysis summary, 2011.

[20] CMS Collaboration, "Search for new physics in events with opposite-sign dileptons and missing transverse energy", cms physics analysis summary, 2011.

[21] C. P. Robert, "The Bayesian Choice: from Decision-Theoretic Foundations to Computational Implementation". Springer Verlag, New York, 2nd ed. edition, 2007.

[22] A. O'Hagan, "Bayesian Inference". Number Vol. 2B in Kendall's Advanced Theory of Statistics. Edward Arnold, London, 1994.

[23] C. F. Berger, J. S. Gainer, J. L. Hewett, and T. G. Rizzo, "Supersymmetry Without Prejudice", *JHEP* **0902** (2009) 023, doi:10.1088/1126-6708/2009/02/023, arXiv:0812.0980.

[24] S. S. AbdusSalam et al., "Fitting the Phenomenological MSSM", *Phys.Rev.* **D81** (2010) 095012, doi:10.1103/PhysRevD.81.095012, arXiv:0904.2548.

[25] J. A. Conley et al., "Supersymmetry Without Prejudice at the LHC", *Eur.Phys.J.* **C71** (2011) 1697, doi:10.1140/epjc/s10052-011-1697-z, arXiv:1009.2539.

[26] J. A. Conley et al., "Supersymmetry Without Prejudice at the 7 TeV LHC", *Physical Review D* (2011) arXiv:1103.1697.

[27] M. Farina et al., "Implications of XENON100 and LHC results for Dark Matter models", *Nucl.Phys.* **B853** (2011) 607–624, doi:10.1016/j.nuclphysb.2011.08.003, arXiv:1104.3572.

[28] A. Arbey, M. Battaglia, and F. Mahmoudi, "Implications of LHC Searches on SUSY Particle Spectra: The pMSSM Parameter Space with Neutralino Dark Matter", *Eur.Phys.J.* **C72** (2012) 1847, doi:10.1140/epjc/s10052-011-1847-3, arXiv:1110.3726.

[29] M. W. Cahill-Rowley et al., "The New Look pMSSM with Neutralino and Gravitino LSPs", *Eur.Phys.J.* **C72** (2012) 2156, doi:10.1140/epjc/s10052-012-2156-1, arXiv:1206.4321.

[30] S. S. AbdusSalam, "LHC-7 supersymmetry search interpretation within the phenomenological MSSM", *Phys.Rev.* **D87** (2013), no. 11, 115012, doi:10.1103/PhysRevD.87.115012, arXiv:1211.0999.

[31] M. W. Cahill-Rowley, J. L. Hewett, A. Ismail, and T. G. Rizzo, "More energy, more searches, but the phenomenological MSSM lives on", *Phys.Rev.* **D88** (2013), no. 3, 035002, doi:10.1103/PhysRevD.88.035002, arXiv:1211.1981.

[32] A. Arbey, M. Battaglia, A. Djouadi, and F. Mahmoudi, "An update on the constraints on the phenomenological MSSM from the new LHC Higgs results", *Phys.Lett.* **B720** (2013) 153–160, doi:10.1016/j.physletb.2013.02.001, arXiv:1211.4004.

[33] M. Cahill-Rowley, J. Hewett, A. Ismail, and T. Rizzo, "pMSSM Studies at the 7, 8 and 14 TeV LHC", arXiv:1307.8444.

[34] M. Cahill-Rowley, J. Hewett, A. Ismail, and T. Rizzo, "Constraints on Higgs Properties and SUSY Partners in the pMSSM", arXiv:1308.0297.

[35] B. Allanach, "SOFTSUSY: a program for calculating supersymmetric spectra", *Comput.Phys.Commun.* **143** (2002) 305–331, doi:10.1016/S0010-4655(01)00460-X, arXiv:hep-ph/0104145.

[36] F. Mahmoudi, "SuperIso v2.3: A Program for calculating flavor physics observables in Supersymmetry", *Comput.Phys.Commun.* **180** (2009) 1579–1613, doi:10.1016/j.cpc.2009.02.017, arXiv:0808.3144.

[37] G. Belanger, F. Boudjema, A. Pukhov, and A. Semenov, "MicrOMEGAs: A Program for calculating the relic density in the MSSM", *Comput.Phys.Commun.* **149** (2002) 103–120, doi:10.1016/S0010-4655(02)00596-9, arXiv:hep-ph/0112278.

[38] G. Belanger, F. Boudjema, A. Pukhov, and A. Semenov, "micrOMEGAs: Version 1.3", *Comput.Phys.Commun.* **174** (2006) 577–604, doi:10.1016/j.cpc.2005.12.005, arXiv:hep-ph/0405253.

[39] G. Belanger, F. Boudjema, A. Pukhov, and A. Semenov, "Dark matter direct detection rate in a generic model with micrOMEGAs 2.2", *Comput.Phys.Commun.* **180** (2009) 747–767, doi:10.1016/j.cpc.2008.11.019, arXiv:0803.2360.

[40] M. Muhlleitner, A. Djouadi, and Y. Mambrini, "SDECAY: A Fortran code for the decays of the supersymmetric particles in the MSSM", *Comput.Phys.Commun.* **168** (2005) 46–70, doi:10.1016/j.cpc.2005.01.012, arXiv:hep-ph/0311167.

[41] A. Djouadi, J. Kalinowski, and M. Spira, "HDECAY: A Program for Higgs boson decays in the standard model and its supersymmetric extension", *Comput.Phys.Commun.* **108** (1998) 56–74, doi:10.1016/S0010-4655(97)00123-9, arXiv:hep-ph/9704448.

[42] P. Z. Skands et al., "SUSY Les Houches accord: Interfacing SUSY spectrum calculators, decay packages, and event generators", *JHEP* **0407** (2004) 036, doi:10.1088/1126-6708/2004/07/036, arXiv:hep-ph/0311123.

[43] Heavy Flavor Averaging Group, "Averages of B-Hadron, C-Hadron, and tau-lepton properties as of early 2012", arXiv:1207.1158.

[44] M. Misiak et al., "Estimate of B(anti-B $\to$ X(s) gamma) at O(alpha(s)^2)", *Phys.Rev.Lett.* **98** (2007) 022002, doi:10.1103/PhysRevLett.98.022002, arXiv:hep-ph/0609232.

[45] HFAG2013. "http://www.slac.stanford.edu/xorg/hfag/rare/2013/radll/OUTPUT/TABLES/radll.pdf.

[46] ATLAS, CMS and LHCb Collaborations, "Search for the rare decays Bs and B0 to dimuons at the LHC with the ATLAS, CMS and LHCb experiments", cms physics analysis summary, 2012.

[47] CMS and LHCb Collaborations, "Combination of results on the rare decays $B^0_{(s)} \to \mu^+\mu^-$ from the CMS and LHCb experiments", cms physics analysis summary, 2013.

[48] Particle Data Group, "Review of particle physics", *J.Phys.* **G37** (2010) 075021, doi:10.1088/0954-3899/37/7A/075021.

[49] K. Hagiwara et al., "$(g-2)_\mu$ and $\alpha(M_Z^2)$ re-evaluated using new precise data", *J.Phys.* **G38** (2011) 085003, doi:10.1088/0954-3899/38/8/085003, arXiv:1105.3149.

[50] CMS Collaboration, "LHC Combination: Top mass", CMS Physics Analysis Summary CMS-PAS-TOP-12-001, 2012.

[51] Tevatron Electroweak Working Group, CDF and D0 Collaborations, "Combination of CDF and DO results on the mass of the top quark using up to 8.7 fb^{-1} at the Tevatron", arXiv:1305.3929.

[52] Joint LEP2 SUSY Working Group, the Aleph, Delphi, L3 and Opal Collaborations. http://lepsusy.web.cern.ch/lepsusy/.

[53] A. A. Markov, "Extension of the limit theorems of probability theory to a sum of variables connected in a chain". reprinted in Appendix B of: R. Howard, *Dynamic Probabilistic Systems, volume 1: Markov Chains*, John Wiley and Sons, 1971.

[54] Metropolis, N. and Rosenbluth, A. W. and Rosenbluth, M. N. and Teller, A. H. and Teller, E., "Equation of State Calculations by Fast Computing Machines", *J. Chem. Phys* **21** (1953) 1087–1092, doi:{10.1063/1.1699114}.

[55] W. K. Hastings, "Monte Carlo sampling methods using Markov chains and their applications", *Biometrika* **57** (1970), no. 1, 97–109, doi:10.1093/biomet/57.1.97.

[56] B. A. Berg, "Markov chain monte carlo simulations and their statistical analysis". World Scientific, 2004.

[57] CMS Collaboration, "Search for new physics in the multijet and missing transverse momentum final state in proton-proton collisions at $\sqrt{s} = 7$ TeV", *Phys.Rev.Lett.* **109** (2012) 171803, doi:10.1103/PhysRevLett.109.171803, arXiv:1207.1898.

[58] CMS Collaboration, "Search for supersymmetry in events with b-quark jets and missing transverse energy in pp collisions at 7 TeV", *Phys.Rev.* **D86** (2012) 072010, doi:10.1103/PhysRevD.86.072010, arXiv:1208.4859.

[59] CMS Collaboration, "Search for electroweak production of charginos and neutralinos using leptonic final states in pp collisions at $\sqrt{s} = 7$ TeV", *JHEP* **1211** (2012) 147, doi:10.1007/JHEP11(2012)147, arXiv:1209.6620.

[60] CMS Collaboration, "Search for new physics in the multijet and missing transverse momentum final state in proton-proton collisions at $\sqrt{s}$ = 8 TeV", cms physics analysis summary, 2014.

[61] CMS Collaboration, "Search for gluino mediated bottom- and top-squark production in multijet final states in pp collisions at 8 TeV", *Phys.Lett.* **B725** (2013) 243–270, doi:10.1016/j.physletb.2013.06.058, arXiv:1305.2390.

[62] CMS Collaboration, "Search for electroweak production of charginos, neutralinos, and sleptons using leptonic final states in pp collisions at 8 TeV", CMS Physics Analysis Summary CMS-PAS-SUS-13-006, 2013.

[63] T. Sjostrand, S. Mrenna, and P. Z. Skands, "PYTHIA 6.4 Physics and Manual", *JHEP* **0605** (2006) 026, doi:10.1088/1126-6708/2006/05/026, arXiv:hep-ph/0603175.

[64] CMS Collaboration, "The fast simulation of the CMS detector at LHC", *J.Phys.Conf.Ser.* **331** (2011) 032049, doi:10.1088/1742-6596/331/3/032049.

[65] P. C. Bhat, H. B. Prosper, and S. S. Snyder, "Bayesian analysis of multisource data", *Phys.Lett.* **B407** (1997) 73–78, doi:10.1016/S0370-2693(97)00723-5.

[66] B. Dumont, J. F. Gunion, and S. Kraml, "The phenomenological MSSM in view of the 125 GeV Higgs data", *Phys.Rev.* **D89** (2014) 055018, doi:10.1103/PhysRevD.89.055018, arXiv:1312.7027.

[67] J. Gunion and H. E. Haber, "Higgs Bosons in Supersymmetric Models. 1.", *Nucl.Phys.* **B272** (1986) doi:10.1016/0550-3213(86)90340-8. [Erratum-ibid. B 402, 567 (1993)].

[68] CMS Collaboration, "Search for neutral Higgs bosons decaying to τ pairs in pp collisions at $\sqrt{s} = 7$ TeV", *Phys.Lett.* **B713** (2012) 68–90, doi:10.1016/j.physletb.2012.05.028, arXiv:1202.4083.

[69] CMS Collaboration, "Higgs to tau tau (MSSM)", CMS Physics Analysis Summary CMS-PAS-HIG-13-021, 2013.

[70] Planck Collaboration, "Planck 2013 results. XVI. Cosmological parameters", arXiv:1303.5076.

[71] LUX Collaboration, "First results from the LUX dark matter experiment at the Sanford Underground Research Facility", arXiv:1310.8214.